J. metamorphic Geol., 2002, **20**, 887–902

Kyanite-paragonite-bearing assemblages, northern Fiordland, New Zealand: rapid cooling of the lower crustal root to a Cretaceous magmatic arc

N. R. DACZKO,[1,*] G. L. CLARKE[1] AND K. A. KLEPEIS[2]
[1]School of Geosciences, FO5, University of Sydney, NSW 2006 Australia (geoffc@mail.usyd.edu.au)
[2]Department of Geology, University of Vermont, Burlington, VT 05405, USA

ABSTRACT Fiordland, New Zealand exposes the lower crustal root of an Early Cretaceous magmatic arc that now forms one of Earth's most extensive high-*P* granulite facies belts. The Arthur River Complex, a dioritic to gabbroic suite in northern Fiordland, is part of the root of the arc, and records an Early Cretaceous history of emplacement, tectonic burial, and high-*P* granulite facies metamorphism that accompanied partial melting of the crust. Late random intergrowths of kyanite, quartz and plagioclase partially pseudomorph minerals in the earlier high-*T* assemblages of the Arthur River Complex, indicating high-*P* cooling of an over thickened crustal root by *c*. 200 °C. The kyanite intergrowths are themselves partially pseudomorphed by paragonite, commonly in the presence of phengitic white mica. Biotite–plagioclase intergrowths that partially pseudomorph phengitic white mica and diopside–plagioclase intergrowths that partially pseudomorph jadeitic diopside, combined with published thermochronology results, are consistent with later rapid decompression. A short duration anticlockwise *P–T* path may be explained by the high-*P* juxtaposition of comparatively cool upper crustal rocks following their tectonic burial and under thrusting during the waning stages of Early Cretaceous orogenesis. This was then followed by the decompression giving the rapid exhumation within 20 Myr of peak metamorphism, as suggested by the isotopic data.

Key words: cooling; high-*P* granulites; magmatic arc; *P–T* path; thermobarometry.

INTRODUCTION

Studies of the deepest levels of young magmatic arcs are important for interpreting the evolution of orogenic belts and environments in which new continental crust is generated. These studies are somewhat hindered by the limited exposure of truly lower crustal rocks (e.g. Miller *et al*., 1993). Plate tectonic models emphasise the importance of large lateral and vertical motions of such arc crust (Whitney *et al*., 1999), drawing on evidence from changes in metamorphic assemblages (Whitney *et al*., 1999; Clarke *et al*., 2000). Rapid increases in metamorphic pressure are mostly ascribed to tectonic thickening and burial during plate convergence (Bradshaw, 1989a; Umhoefer & Miller, 1996). Rapid increases in metamorphic temperature are commonly ascribed to magmatic activity, pronounced cooling to tectonic stabilisation, and the termination of metamorphism is most commonly associated with rapid exhumation (e.g. Monie *et al*., 1994; Treloar, 1997). We have discovered a range of Cretaceous assemblages in northern Fiordland, New Zealand, that superficially contrast with some of the common tectonic interpretations.

Perhaps the most striking metamorphic feature that has been described in gabbroic rocks from Fiordland involves garnet–clinopyroxene-bearing corona reaction textures that mantle enstatite and hornblende in garnet reaction zones. These reflect *c*. 25 km of burial of an Early Cretaceous granulite facies terrane (Clarke *et al*., 2000). Large garnet poikiloblasts that are surrounded by leucosome in dioritic components of the Arthur River Complex reflect high-*P* crustal anatexis that postdates burial (Daczko *et al*., 2001b). In this paper, we describe high-*P* amphibolite facies assemblages involving kyanite, paragonite and phengitic white mica (hereafter referred to as phengite) that partially pseudomorph the granulite facies minerals and reflect rapid high-*P* cooling of the rocks by *c*. 200 °C. Biotite–plagioclase-bearing intergrowths that partially pseudomorph phengite, and textures involving the breakdown of jadeitic diopside to diopside-plagioclase intergrowths, developed during decompression (e.g. Franz *et al*., 1986; Elveold & Gilotti, 2000) that followed the rapid cooling. The high-*P* amphibolite facies assemblages indicate that the northern Fiordland rocks cooled substantially prior to the onset of extension that led to the unroofing of the root of the arc during the mid-Cretaceous (cf. Gibson *et al*., 1988; Tulloch & Kimbrough, 1989).

* Now at: Jackson School of Geosciences, The University of Texas at Austin, Austin, Texas, TX 78712, USA.

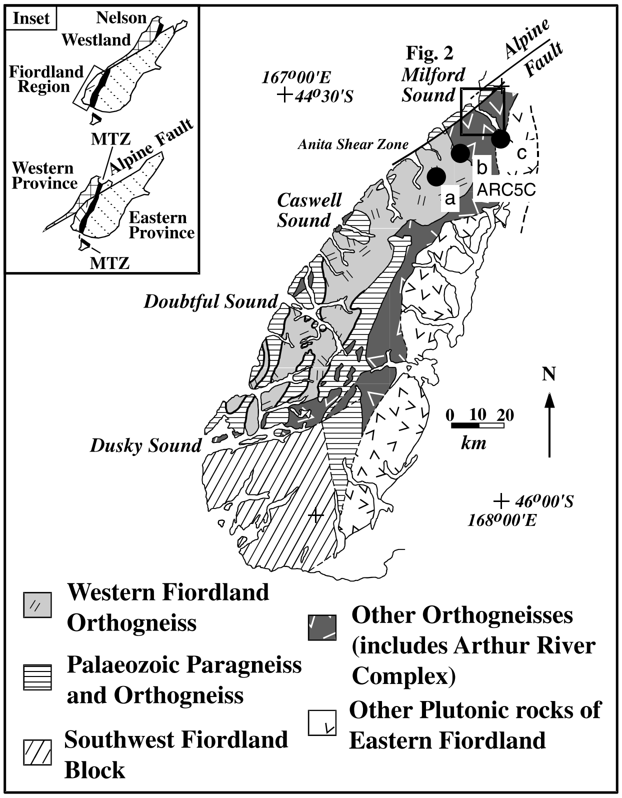

Fig. 1. Geological map of Fiordland showing major lithological divisions (after Bradshaw, 1990). Inset shows the pre-Cenozoic configuration of the South Island, which places the Westland-Nelson region adjacent to Fiordland. Black filled circle labelled 'a' is the site of geochronological data 1, 2 and 3 in Table 2. Black filled circle labelled 'b' marks the site of sample ARC5C. Black circle labelled 'c' is the site of geochronological data 15, 16, and 17 in Table 2.

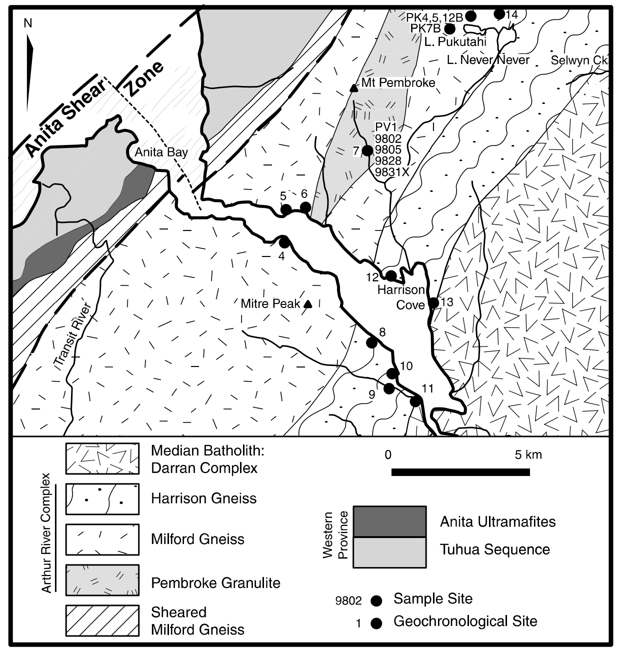

Fig. 2. Geological Map of the Milford Sound area (after Wood, 1972; Blattner, 1991; Hill, 1995a; Clarke *et al*., 2000). Black filled circles mark sample sites or the sites of geochronological data 4–14 in Table 2.

REGIONAL GEOLOGY

The geology of the south island of New Zealand can be divided into three domains. The Eastern and Western Provinces (Landis & Coombs, 1967; Bishop *et al*., 1985; inset Fig. 1) are separated by a belt of rocks referred to as the Median Tectonic Zone (Kimbrough *et al*., 1993, 1994; inset Fig. 1) or Median Batholith (Mortimer *et al*., 1999). The Western Province contains mostly Lower Palaeozoic paragneiss, cut by Devonian, Carboniferous and Cretaceous granitoids (Muir *et al*., 1996; Wandres *et al*., 1998). It includes the Arthur River Complex (Bradshaw, 1990; Figs 1 & 2), a belt of granulite facies orthogneiss that lies at the boundary between the Median Tectonic Zone and Western Province rocks in northern Fiordland (Fig. 1). It is heterogeneous in rock-type and structure (Clarke *et al*., 2000). Recent geochronological studies indicate Mesozoic and Palaeozoic ages for orthogneiss units from this belt (Mattinson *et al*., 1986; Bradshaw, 1990; Tulloch *et al*., 2000), suggesting it contains both Median Batholith and Western Province components (Tulloch *et al*., 2000). In Milford Sound, the Arthur River Complex includes dioritic and gabbroic gneisses of the Harrison Gneiss, Pembroke Granulite and Milford Gneiss (Fig. 2; Wood, 1972; Blattner, 1978, 1991; Clarke *et al*., 2000). The Anita Shear Zone forms the northwestern boundary of the Arthur River Complex; Palaeozoic paragneiss of the Western Province lie north-west of the shear zone (Fig. 2; Hill, 1995a,b; Klepeis *et al*., 1999). The Late Jurassic to Early Cretaceous (*c*. 147–137 Ma) Darran Complex, named after the Darran Diorite (Wood, 1972; Bradshaw, 1990; Kimbrough *et al*., 1994), lies to the east of the Arthur River Complex and forms part of the Median Batholith (Fig. 2). The boundary between these two units has been proposed as a faulted contact (Koons, 1978; Bradshaw, 1990) or as a strain gradient (Blattner, 1991; Clarke *et al*., 2000). The 126–119 Ma Western Fiordland Orthogneiss intrudes the Arthur River Complex, 19 km southwest of Milford Sound at Mt Daniel (Bradshaw, 1990).

Structural and Metamorphic overview

The Arthur River Complex, exposed in northern Fiordland, contains high-*P* granulite facies dioritic to gabbroic rocks that experienced at least five deformation events in the Early Cretaceous (Blattner, 1991; Clarke *et al*., 2000; Daczko *et al*., 2001a). The following overview of the structural and metamorphic history of the Arthur River Complex is a summary of data presented by Clarke *et al*. (2000), Daczko *et al*. (2001a,b). A summary of structural abbreviations is provided in Table 1. The earliest foliation (S1), preserved in the Pembroke Granulite, is defined by two-pyroxene–hornblende-bearing granulite

Table 1. Summary of structural and metamorphic events referred to in text.

Event	Structure	Metamorphism	Reference
D1 – S1	Pervasive S1-L1 two-pyroxene-hornblende fabric in Pembroke Granulite	< 8 kbar, > 750 °C	Clarke *et al.* (2000)
D2 – Grt reaction zones	Partial melting, fracturing, trondhjemitic veining and garnet reaction zone development	= 14 kbar, = 750–850 °C	Daczko *et al.* (2001b)
D3 – S3	Pervasive S3-L3 fabric in narrow steeply dipping mylonites	= 14 kbar, ≈ 700 °C	Daczko *et al.* (2001a)
D4 – S4	Thrust faults in Pembroke Granulite, Pervasive S4-L4 steeply dipping fabric in Milford Gneiss	> 12 kbar, = 600–700 °C	Daczko *et al.* (2001a) This study
Ky-Pg-Phg assemblages	Random in Pembroke Granulite Aligned with S4 in Milford Gneiss	= 11–13 kbar, = 600–700 °C	This study
ASZ1	Pervasive shallowly dipping fabric (ductile normal fault) in Anita Shear Zone	≈ 12 kbar, ≈ 600 °C	Klepeis *et al.* (1999)
Phg Breakdown	Pseudomorphous replacement of phengite by biotite	< 12 kbar?, ≈ 600 °C	This study
Post-D4 Pegmatites	Pegmatites with garnet-biotite-phengite-bearing selvage	≈ 9 kbar, ≈ 600 °C	This study
ASZ2	Pervasive steeply dipping fabric (dextral transpression) in Anita Shear Zone	≈ 9 kbar, ≈ 600 °C	Klepeis *et al.* (1999)

facies assemblages. S1 generally strikes east to east-north-east and displays steep to near-vertical dips to the south and SSE. A weakly developed mineral lineation plunges variably to the east and west. S1 mineral assemblages reflect conditions of < 8 kbar and > 750 °C. S1 is cut by steeply dipping planar fractures (D2) that are commonly filled by trondhjemitic veins. In dioritic gneiss, the veins are linked to large garnet poikiloblasts, commonly surrounded by leucosome. These textures reflect high-*P* partial melting of dioritic gneiss at T > 750 °C. Gabbroic gneiss, in contact with the dioritic gneiss, shows no evidence of partial melting. However, adjacent and parallel to the D2 fractures and veins in gabbroic gneiss, S1 minerals are pseudomorphed by garnet–clinopyroxene-bearing assemblages in what are referred to as garnet reaction zones (Blattner, 1976; Oliver, 1977; Bradshaw, 1989b). Assemblages in the garnet reaction zones record metamorphic conditions of 12–14 kbar and 750–850 °C. S1 and the garnet reaction zones were deformed by two phases of collisional-style granulite facies deformation at lower crustal conditions. A series of approximately 1 m wide shear zones (D3) formed within a pure-shear-dominated sinistral regime that led to bulk horizontal shortening and NE–SW stretching. D4 thrust faults in the Pembroke Granulite and a north-striking, steeply dipping foliation (S4) in the Milford and Harrison Gneisses cut the D3 shear zones. The development of S4 was accompanied by partial rehydration and appreciable cooling, as temperature conditions evolved from being above or close to the fluid-undersaturated diorite solidus (D2) to those that enabled retrograde white mica growth (Daczko *et al.*, 2001b). Hydrous fluid ingress at peak conditions would have initiated appreciable partial melting in all rocks (e.g. Johannes & Holtz, 1991). Throughout Milford Sound, S4 shows variable mineral assemblages in rocks of similar composition, reflecting D4 deformation over a wide range of temperatures. For example, sample 9608c contains the S4 assemblage garnet, clinopyroxene, hornblende, plagioclase and quartz that give garnet-clinopyroxene thermometry estimates of 800 °C (Table 2 in Clarke *et al.*, 2000). However, more hydrous S4 paragonite-phengite-bearing assemblages presented here reflect conditions of $T = 600$–700 °C and indicate that either: (i) S4 developed over some period of time during cooling and hydration; or (ii) S4 experienced reactivation following cooling and hydration. Fabrics of the Anita Shear Zone that are related to exhumation of the high-*P* rocks cut S4 further west (Klepeis *et al.*, 1999).

Table 2. Geochronological data.

Site	Easting	Northing	Dated material	Geological Unit	Dating Method	Reported Age (Ma)	Error ± (Ma)	Reference
1	2086700	5580027	apatite	WFO	U-Pb	92.6	2.0	Mattinson *et al.* (1986)
	2086700	5580027	apatite	WFO	U-Pb	91.0	2.0	Mattinson *et al.* (1986)
	2086700	5580027	zircon	WFO	U-Pb	120–130		Mattinson *et al.* (1986)
2	2090891	5575534	apatite	WFO	U-Pb	89.3	0.5	Mattinson *et al.* (1986)
3	2091969	5586789	zircon	WFO	U-Pb	125.9	1.9	Muir *et al.* (1998)
4	2101621	5608980	hornblende	Milford Gneiss	K-Ar	90.3	2.6	Nathan *et al.* (2000)
5	2101970	5609899	plagioclase	Milford Gneiss	K-Ar	113.4	1.8	Nathan *et al.* (2000)
	2101970	5609899	hornblende	Milford Gneiss	K-Ar	111.0	2.0	Nathan *et al.* (2000)
	2101970	5609899	muscovite	Pegmatite	K-Ar	30.8	0.8	Nathan *et al.* (2000)
6	2102800	5609456	hornblende	Milford Gneiss	K-Ar	104.8	0.8	Nathan *et al.* (2000)
	2102800	5609456	hornblende	Milford Gneiss	K-Ar	105.0	4.0	Nathan *et al.* (2000)
7	2104300	5612300	hornblende	Pembroke Granulites	K-Ar	137.5	1.0	Nathan *et al.* (2000)
	2104300	5612300	hornblende	Pembroke Granulites	K-Ar	138.0	4.0	Nathan *et al.* (2000)
8	2104515	5605559	hornblende	Harrison Gneiss	K-Ar	92.3	2.8	Nathan *et al.* (2000)
9	2104658	5602438	muscovite	Harrison Gneiss	K-Ar	25.2	0.8	Nathan *et al.* (2000)
10	2105634	5604300	muscovite	Harrison Gneiss	K-Ar	68.9	1.8	Nathan *et al.* (2000)
	2105634	5604300	hornblende	Harrison Gneiss	K-Ar	149.0	4.0	Nathan *et al.* (2000)
11	2106476	5603218	hornblende	Harrison Gneiss	K-Ar	91.0	0.4	Nathan *et al.* (2000)
12	2104200	5608100	zircon	Milford Gneiss	U-Pb	355	10.0	Tulloch *et al.* (2000)
						134	2.0	
						120	2.0	
13	2106778	5606695	hornblende	Harrison Gneiss	K-Ar	164.0	4.0	Nathan *et al.* (2000)
	2106778	5606695	muscovite	Harrison Gneiss	K-Ar	67.7	1.8	Nathan *et al.* (2000)
14	2108977	5616603	hornblende	Milford Gneiss	K-Ar	84.5	2.6	Nathan *et al.* (2000)
	2108977	5616603	hornblende	Milford Gneiss	K-Ar	74.0	2.4	Nathan *et al.* (2000)
	2108977	5616603	plagioclase	Milford Gneiss	K-Ar	62.2	1.8	Nathan *et al.* (2000)
15	2110731	5595164	hornblende	Darran Complex	K-Ar	153.0	8.0	Nathan *et al.* (2000)
	2110731	5595164	hornblende	Darran Complex	K-Ar	153.0	4.0	Nathan *et al.* (2000)
16	2114480	5594957	biotite	Darran Complex	K-Ar	134.0	4.0	Nathan *et al.* (2000)
	2114480	5594957	hornblende	Darran Complex	K-Ar	142.0	4.0	Nathan *et al.* (2000)
17	2111641	5600479	zircon	Darran Complex	U-Pb	137.0	1.0	Mattinson *et al.* (1986)
	2111641	5600479	apatite	Darran Complex	U-Pb	113.0	0.4	Mattinson *et al.* (1986)

Geochronological overview

U–Pb zircon ion probe analyses distinguish three age populations for a single sample of the Arthur River Complex: (1) large Palaeozoic oscillatory zoned cores yield an age of 355 ± 10 Ma; (2) large Early Cretaceous cores with sector zoning yield an age of 134 ± 2 Ma; and (3) low-U zircon rims (on both Palaeozoic and Cretaceous cores) with an average age of 120 Ma (Tulloch *et al.*, 2000). The data allow for a Palaeozoic or Early Cretaceous protolith for the Arthur River Complex orthogneisses. The metamorphic rims on zircon grains suggest that peak metamorphism occurred at *c.* 120 Ma. These data compare well with timing constraints made on the basis of fabric development that suggest that all fabrics in the Arthur River Complex post date emplacement of the Western Fiordland Orthogneiss at 126–119 Ma (Clarke *et al.*, 2000). The peak metamorphism in the Arthur River Complex coincides with the final stages of Western Fiordland Orthogneiss emplacement.

K–Ar isotopic dating of hornblende grains from the Pembroke Granulite yield ages of *c.* 138 Ma (Table 2; Nathan *et al.*, 2000). K–Ar ages for hornblende grains from the Milford and Harrison Gneisses give ages of *c.* 111–90 Ma (Table 2, Nathan *et al.*, 2000), consistent with rapid cooling of the Arthur River Complex by *c.* 90 Ma. Therefore, the Arthur River Complex shows a similar geochronological history to the Western Fiordland Orthogneiss, which was emplaced between 126 and 119 Ma, buried and metamorphosed at high-*P* granulite facies conditions, and, on the basis of U-Pb apatite dates, had cooled to < 300–400 °C by *c.* 90 Ma (Table 2, Mattinson *et al.*, 1986).

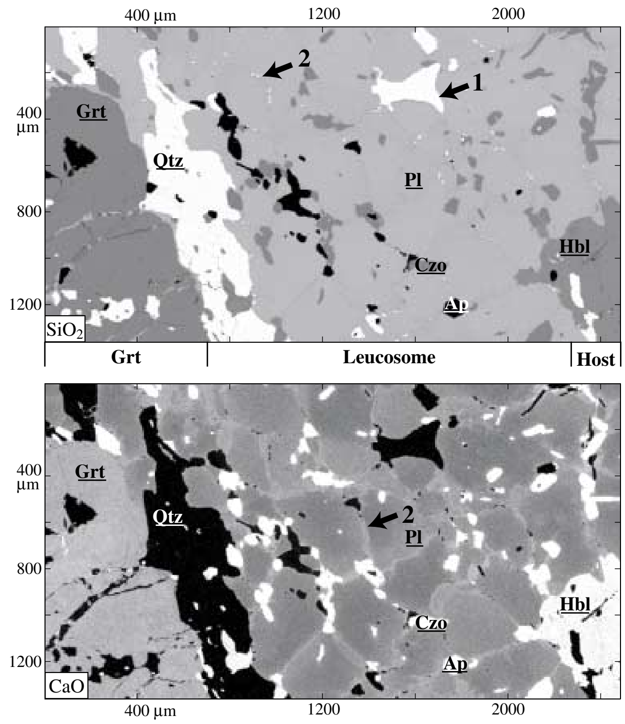

Fig. 3. Matrix corrected maps of oxide weight percent for SiO_2 and CaO (dioritic gneiss sample of the Pembroke Granulite – 9805). The maps cover an area approximately 1300 × 2400 μm. Grey scale is black for minimum elemental concentration and white for maximum elemental concentration. Minimum and maximum ranges: SiO_2 is 0–100 wt.%, CaO is 0–10 wt.%. Arrow labelled with '1' points to quadrangular quartz grain with concave sides. Arrows labelled with '2' point to quartz films along grain boundaries in the SiO_2 map and plagioclase films along grain boundaries on the CaO map.

PETROLOGY

In this section, we describe the petrology of the textures inferred to represent former sites of partial melting, textures involving kyanite-paragonite-phengite-bearing assemblages, and textures involving the breakdown of jadeitic diopside that are useful for estimating the postpeak metamorphic *P–T* path for the Arthur River Complex. Petrographic observations were supplemented with maps of oxide weight percent obtained by applying matrix corrections to raw intensity X-ray maps. All microprobe data were collected on a Cameca SX50 microprobe at the University of New South Wales. Eight X-ray intensity maps were collected in two sessions using four wavelength dispersive spectrometers, with an accelerating voltage of 15 kV, a beam current of 20 nA and a beam width of 1–3 μm. The element maps were collected with a 300-ms count time at each point and a 4-μm step size between points. The raw intensity maps were converted to maps of oxide weight percent by using the α-factor approach of Bence & Albee (1968) for matrix correction (Clarke *et al.*, 2001).

Partial melting textures

Samples of dioritic gneiss from the Pembroke Granulite (e.g. 9802, 9805 and 9831X) have large garnet poikiloblasts (up to 25 mm across) surrounded by leucosome that cuts S1. The garnet poikiloblasts and leucosomes are interpreted by Daczko *et al.* (2001b) to represent sites of partial melting in the dioritic gneiss at T > 750 °C. Textures within the leucosomes (sample 9805; Fig. 3) are consistent with the interpretation that the dioritic gneiss partially melted, using the microstructural criteria of Sawyer, 1999). Figure 3 shows maps of silica and calcium oxide weight percent for sample 9805. The figure shows part of a large garnet poikiloblast on the left, surrounded by leucosome in the centre of the figure, with partially melted dioritic gneiss on the right. The large garnet poikiloblasts mostly contain inclusions of quartz, with or without minor hornblende, clinozoisite, rutile and apatite. The leucosome consists of plagioclase and quartz and contains rounded grains of clinozoisite and hornblende. Quartz commonly shows quadrangular shapes with concave sides (arrow 1, Fig. 3). Quartz and plagioclase grains show no evidence of strain such as recrystallized grain margins or undulose extinction, consistent with these samples experiencing little ductile deformation associated with or following the partial melting. Thin films of quartz and plagioclase occur along some larger plagioclase grain boundaries in the leucosome (arrow 2, Fig. 3). The films of plagioclase (arrow 2 in the CaO map in Fig. 3) are commonly zoned, up to 50 μm across, and are more calcic than the rest of the plagioclase in the leucosome (see later).

Kyanite and paragonite (± phengite) bearing textures

Dioritic gneiss samples 9802, 9805 (outside the area shown in Fig. 3) and 9831X have intergrowths of kyanite, quartz and plagioclase that cut S1 and postdate formation of the leucosomes. The kyanite-bearing intergrowths (up to 3 mm across) are random in orientation and display irregular grain shape with cuspate boundaries. Figure 4 shows maps of Si, Al, Ca and Na oxide weight percent for a kyanite-bearing intergrowth in sample 9831X. Kyanite is generally found armoured by plagioclase and separated from the rest of the rock by areas of quartz (Fig. 4). The kyanite-bearing intergrowths may contain inclusions of hornblende (arrow 1, Fig. 4), clinozoisite, rutile and apatite. In thin section, the intergrowths of kyanite, quartz and plagioclase display curved and irregular grain boundaries with S1 plagioclase and hornblende (Fig. 5a). Many kyanite-bearing intergrowths contain hornblende inclusions suggesting that coarse-grained S1 plagioclase was replaced by the intergrowths before S1 hornblende (Fig. 5b), suggesting:

$$\text{plagioclase}_1 = \text{kyanite} + \text{quartz}\,(+\,\text{minor plagioclase}_2) \qquad (1)$$

A second interpretation of the kyanite-bearing textures is that they represent relict kyanite crystals partially replaced by plagioclase

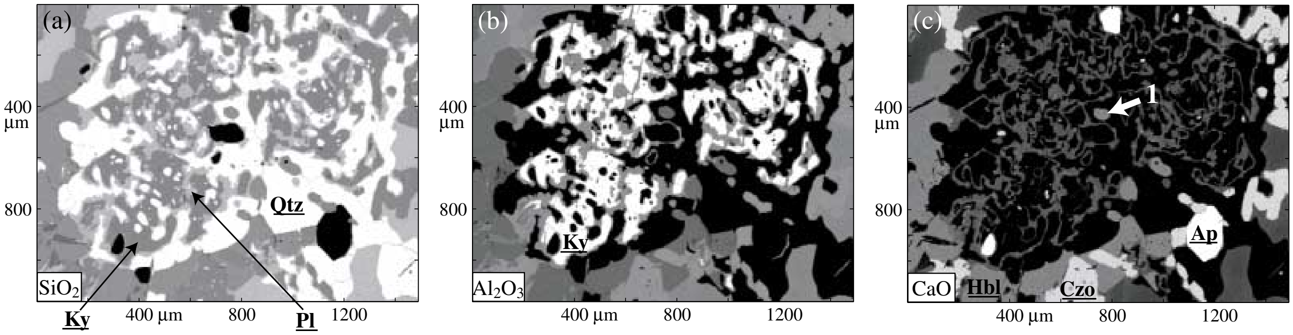

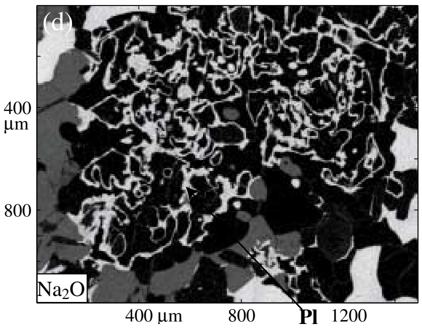

Fig. 4. Matrix corrected maps of oxide weight percent for SiO_2, Al_2O_3, CaO and Na_2O of a kyanite, quartz and plagioclase intergrowth in sample 9831X. The maps cover an area approximately 1000 × 1500 μm. Grey scale is black for minimum elemental concentration and white for maximum elemental concentration. Minimum and maximum ranges: SiO_2 is 0–100 wt.%, Al_2O_3 is 0–63 wt.%, CaO is 0–28 wt.%, Na_2O is 0–13 wt.%. The white mineral is kyanite. The brightest mineral on the Na_2O map is plagioclase. Arrow labelled with '1' points to a hornblende inclusion within the intergrowth.

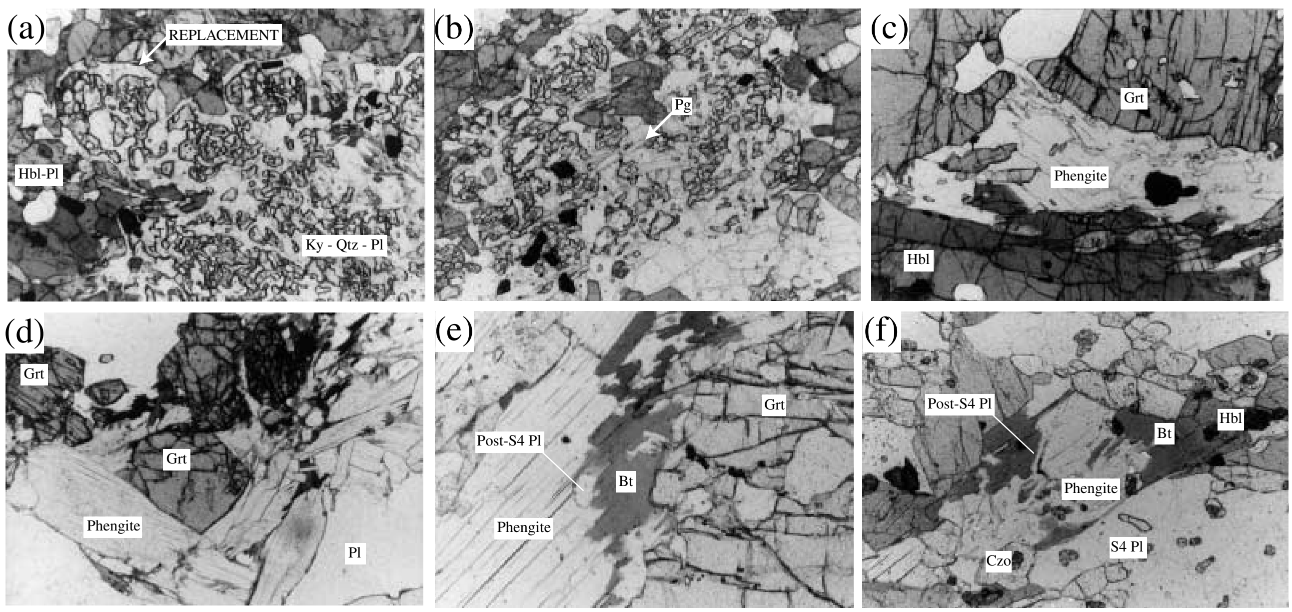

Fig. 5. (a) Photomicrograph of intergrowths of kyanite, quartz and plagioclase after S1 plagioclase and hornblende in sample PV1. Field of view 2.8 mm (b) Photomicrograph of paragonite (± phengite) grains that replace the kyanite-bearing intergrowths in sample 9802. Field of view 2.8 mm. (c) Photomicrograph of paragonite and phengite replacing the rim of a garnet grain in sample PK12B. Field of view 2.8 mm. (d) Photomicrograph of garnet and phengite in the selvage adjacent to a post-D4 pegmatite (sample PK7B). Field of view 2.8 mm. (e) Photomicrograph of biotite partially pseudomorphing phengite adjacent to garnet in sample 9831X. Field of view 1.4 mm. (f) Photomicrograph of biotite and plagioclase after phengite adjacent to hornblende in sample 9831X. Field of view 1.4 mm.

concurrent with partial replacement of hornblende at the contact with former kyanite. We prefer the interpretation that kyanite is intergrown with the plagioclase and quartz and that the intergrowths are late and cut S1 and the leucosomes for the following reasons. The kyanite-bearing intergrowths occur in intensely foliated rock, but are random in orientation, consistent with post-S1 formation. The intergrowths have very irregular boundaries, inconsistent with any shape that could be expected for a relict kyanite grain. The intergrowths entrain rounded grains of plagioclase and hornblende, consistent with the interpretation that they are partially pseudo-

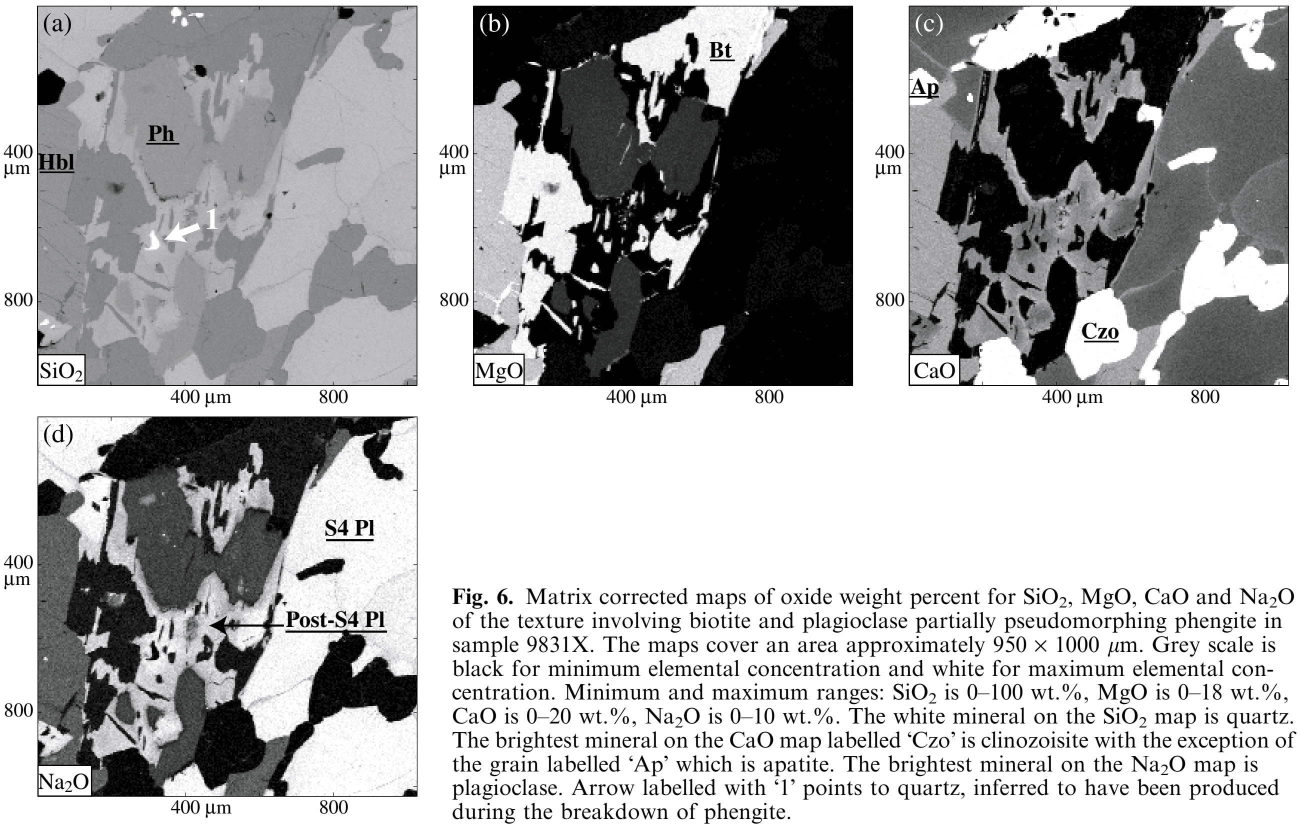

Fig. 6. Matrix corrected maps of oxide weight percent for SiO_2, MgO, CaO and Na_2O of the texture involving biotite and plagioclase partially pseudomorphing phengite in sample 9831X. The maps cover an area approximately 950 × 1000 μm. Grey scale is black for minimum elemental concentration and white for maximum elemental concentration. Minimum and maximum ranges: SiO_2 is 0–100 wt.%, MgO is 0–18 wt.%, CaO is 0–20 wt.%, Na_2O is 0–10 wt.%. The white mineral on the SiO_2 map is quartz. The brightest mineral on the CaO map labelled 'Czo' is clinozoisite with the exception of the grain labelled 'Ap' which is apatite. The brightest mineral on the Na_2O map is plagioclase. Arrow labelled with '1' points to quartz, inferred to have been produced during the breakdown of phengite.

morphing S1 plagioclase and hornblende. In general, there is excellent preservation of earlier textures in low strain zones within the orthogneiss, and nowhere has kyanite been observed as a relict grain. The intergrowths are substantially richer in quartz than the surrounding dioritic gneiss. This is inconsistent with them being relict kyanite grains that were partially replaced by plagioclase as this would require a large influx of silica into the texture. Our preferred interpretation is consistent with the excess silica being formed as plagioclase was replaced by kyanite.

Paragonite, with or without phengite, cuts the kyanite intergrowths in the Pembroke Granulite (Fig. 5b) and may define S4 in the Milford Gneiss (Fig. 5c). Grains of paragonite and phengite in low-D4 strain zones of the Pembroke Granulite are mostly randomly oriented and may be up to 4 mm long. They are most commonly observed in plagioclase. Paragonite and phengite in high-D4 strain zones of the Milford Gneiss are most commonly aligned with S4 hornblende, plagioclase, clinozoisite, garnet and quartz. Figure 5(c) covers an area with S4 paragonite and phengite that partly replace garnet in sample PK12B from the northern side of Lake Pukutahi (Fig. 2).

Post-D4 textures

S4 is cut by muscovite-bearing pegmatites with metasomatic selvages that penetrate the host rock for approximately 5 mm around the pegmatite. The selvages mostly contain garnet, biotite and phengite with plagioclase and quartz (Fig. 5d). This assemblage is useful in that it allows the metamorphic conditions that followed D4 and accompanied the emplacement of the pegmatite to be estimated.

The rims of some S4 phengite grains are pseudomorphed by biotite with or without plagioclase, in samples of both the Pembroke Granulite and Milford Gneiss. This texture is most common where the phengite is in contact with a ferro-magnesian mineral such as garnet or hornblende (Fig. 5e,f). In textures where the pseudomorphous replacement of a phengite grain is almost complete, biotite is observed with plagioclase and minor quartz and potassium feldspar (Fig. 5f). Biotite in the texture is best developed along grain boundaries where phengite is inferred to have been in contact with hornblende. Biotite is least developed where phengite is inferred to have been in contact with coarse-grained plagioclase and clinozoisite. Post-S4 plagioclase in these textures is commonly observed to separate phengite and biotite (Fig. 5e,f). Figure 6 shows maps of silica, magnesium, calcium and sodium oxide weight percent for the texture shown in Fig. 5(f). The figure shows that quartz is a minor product (arrow 1, Fig. 6) and that the anorthite content of the post-S4 plagioclase is higher than that of S4 plagioclase (see later). This suggests that the breakdown of phengite in the presence of hornblende or garnet produced excess Ca that was taken up in the post-S4 plagioclase intergrown with the biotite, suggesting the reaction:

$$\text{phengite} + \text{hornblende (or garnet)} = \text{biotite} + \text{plagioclase} \quad (+ \text{minor quartz, K-feldspar}) \qquad (2)$$

Sample ARC5C is a garnet-clinopyroxene mafic hornfels from the Arthur River Complex at Mt Daniel (Fig. 1). The Arthur River Complex is intruded by the Western Fiordland Orthogneiss batholith at Mt Daniel and sample ARC5C is located in the contact areole of the batholith (Daczko *et al.* in press). The sample contains textures important to the postpeak, *P–T* path, rare amongst the garnet-clinopyroxene hornfels in that area as it contains coarse-grained plagioclase with the peak assemblage of garnet, jadeitic diopside, hornblende, quartz and rutile. This assemblage is used below to infer peak metamorphic conditions for this area of the Arthur River Complex. Figure 7 shows maps of silica, aluminium, calcium and sodium oxide weight percent for sample ARC5C. The maps show coarse-grained garnet, jadeitic diopside, plagioclase and quartz. The rims of the jadeitic diopside have been replaced by fine-grained intergrowths of diopside and plagioclase (arrow 1, Fig. 7), suggesting the reaction:

$$\text{jadeitic diopside} = \text{diopside} + \text{plagioclase} \qquad (3)$$

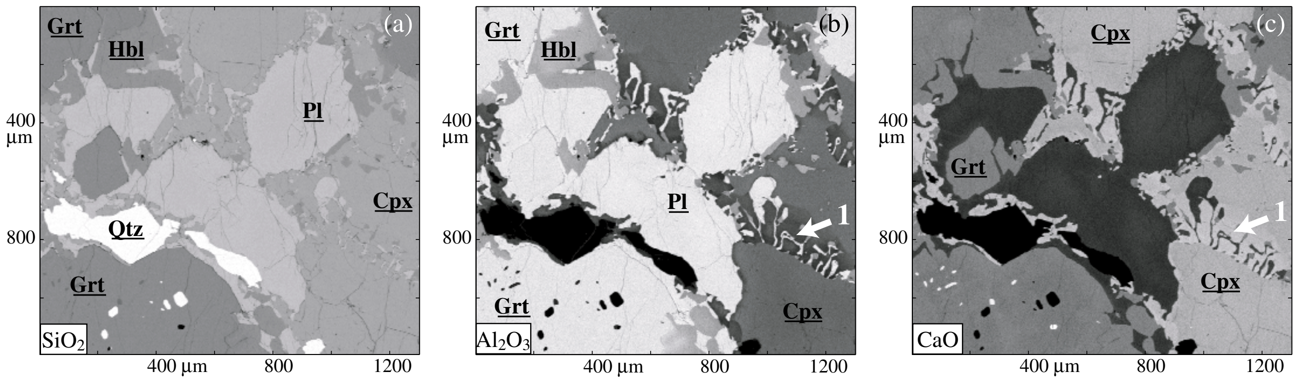

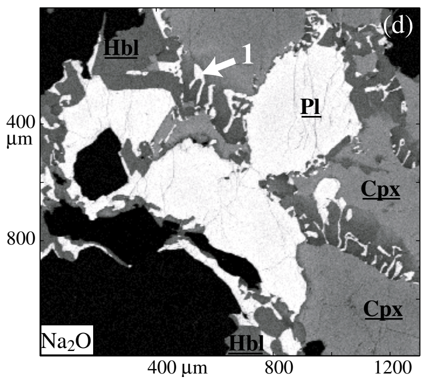

Fig. 7. Matrix corrected maps of oxide weight percent for SiO_2, Al_2O_3, CaO and Na_2O over the texture involving diopside and plagioclase partially pseudomorphing jadeitic diopside in sample ARC5C. The maps cover an area approximately 1150 × 1300 μm. Grey scale is black for minimum elemental concentration and white for maximum elemental concentration. Minimum and maximum ranges: SiO_2 is 0–100 wt.%, Al_2O_3 is 0–27 wt.%, CaO is 0–35 wt.%, Na_2O is 0–11 wt.%. Arrow labelled with '1' points to plagioclase and diopside intergrowths, inferred to have been produced during the breakdown of jadeitic diopside.

MINERAL CHEMISTRY

Mineral chemistries of the textures described above are used to estimate metamorphic conditions that accompanied the development of the textures. Representative electron microprobe analyses of minerals used in *P–T* calculations are presented in Table 3. Data were collected on a Cameca SX50 electron microprobe at the University of New South Wales with an accelerating voltage of 15 kV, a beam current of 20 nA and a beam width of 1–3 μm.

There are four textural varieties of garnet in samples of the Arthur River Complex discussed in this paper: (i) large garnet poikiloblasts from former sites of partial melting (Fig. 3); (ii) garnet within S4 (Fig. 5c,e); (iii) garnet in metasomatic selvages associated with post-D4 pegmatites (Fig. 5d); and (iv) in the garnet-clinopyroxene hornfels from the Western Fiordland Orthogneiss contact aureole at Mt Daniel (Fig. 7). No two textural varieties are found in the same sample. Large garnet poikiloblasts from sites of former partial melting in dioritic gneiss of the Pembroke Granulite (samples 9802, 9805 & 9831X) are unzoned pyrope- and grossular-rich almandine with $Alm_{56}Sps_2Py_{25}Gr_{17}$ where Alm = 100Fe/(Fe + Mg + Mn + Ca), Sps = 100Mn/(Fe + Mg + Mn + Ca), Py = 100Mg/(Fe + Mg + Mn + Ca) and Gr = 100Ca/(Fe + Mg + Mn + Ca). S4 garnet has a variable composition in the range $Alm_{53-70}Sps_{0-3}Py_{14-27}Gr_{15-26}$. This variability most probably reflects minor variability in whole rock compositions across the dioritic to gabbroic suite of the Arthur River Complex. Individual garnet grains within S4 are most commonly unzoned. However, garnet in sample PK5 is unusual and shows bell-shaped zoning profiles with a core composition of $Alm_{56}Sps_6Py_{13}Gr_{25}$ and a rim composition of $Alm_{59}Sps_3Py_{19}Gr_{19}$. Garnet in the metasomatic selvage adjacent to the post-D4 pegmatite has a variable composition in the range $Alm_{59-61}Sps_{6-11}Py_{9-15}Gr_{18-24}$. Garnet in the garnet-clinopyroxene hornfels at Mt Daniel is unzoned pyrope- and grossular-rich almandine with $Alm_{43}Sps_1Py_{25}Gr_{30}$. Garnet microprobe analyses from all dioritic and gabbroic samples plot in a similar region on a ternary diagram (Fig. 8a). The overall trend on Fig. 8(a) implies exchange vectors involving Ca ↔ Mg or (Fe, Ca) ↔ 2 Mg in garnet.

There are seven textural varieties of plagioclase in samples of the Arthur River Complex discussed in this paper: (i) plagioclase within leucosome from sites of former partial melting (Fig. 3 middle); (ii) plagioclase in dioritic gneiss that hosts sites of former partial melting (outside leucosome, Fig. 3 far right); (iii) plagioclase associated with kyanite intergrowths (Figs 4, 5a,b); (iv) plagioclase within S4 (Figs 5c,f, & 6); (v) plagioclase intergrown with biotite at sites of former phengite breakdown (Figs 5f & 6); (vi) coarse-grained plagioclase from the garnet-clinopyroxene hornfels at Mt Daniel (Fig. 7); and (vii) fine-grained plagioclase intergrown with diopside at former sites of jadeitic diopside breakdown at Mt Daniel (Fig. 7). Plagioclase within leucosome from sites of former partial melting is oligoclase to andesine with

Table 3. Representative microprobe analyses (wt% oxide and cation data).

	9831X (cooling)					9828 (hydration)					PK5 (S4)			ARC5C (peak)							
	Grt	Hbl	Pl	Czo	Ky	Grt	Hbl	Pl	Czo	Pg	Grt	Hbl	Pl	Czo	Pg	Grt	Jadeitic Di		Pl	Hbl	Di
SiO_2	38.5	42.3	63.7	38.4	36.8	38.4	41.6	63.1	38.6	46.2	38.3	42.2	63.1	38.3	45.9	38.3	52.2		63.8	42.0	52.5
TiO_2	0.0	0.6	0.0	0.1	0.0	0.1	0.7	0.0	0.2	0.2	0.0	0.5	0.0	0.1	0.3	0.0	0.4		0.0	1.1	0.3
Al_2O_3	21.7	16.2	22.8	27.0	62.1	21.2	17.3	23.4	27.3	39.4	21.5	16.5	23.1	27.1	38.9	21.7	6.0		23.1	15.0	1.9
Cr_2O_3	0.0	10.8	0.0	0.0	0.0	0.0	0.0	0.0	0.0	0.0	0.0	0.0	0.0	0.0	0.0	0.1	0.0		0.0	0.0	0.0
FeO	26.6	14.3	0.1	7.9	0.8	27.2	14.0	0.1	7.4	0.9	27.0	14.9	0.0	8.0	0.9	22.3	7.6		0.1	13.7	7.6
MnO	1.1	0.1	0.0	0.0	0.0	1.3	0.1	0.0	0.0	0.0	1.2	0.2	0.0	0.1	0.0	0.4	0.0		0.0	0.1	0.1
MgO	6.3	0.0	0.0	0.0	0.0	5.3	10.0	0.0	0.0	0.1	5.3	9.8	0.0	0.1	0.1	5.4	11.1		0.0	10.8	13.0
CaO	5.8	10.5	4.4	23.2	0.0	6.7	10.3	4.6	22.9	0.5	6.9	10.1	4.2	23.3	0.5	11.8	19.8		4.0	10.6	22.9
Na_2O	0.0	2.1	9.3	0.0	0.0	0.0	2.7	9.1	0.0	7.0	0.0	2.2	9.1	0.0	6.6	0.0	3.1		9.3	2.7	1.1
K_2O	0.0	0.6	0.1	0.0	0.0	0.0	0.5	0.1	0.0	1.1	0.0	0.4	0.1	0.0	1.1	0.0	0.0		0.1	1.2	0.0
Total	100.1	97.5	100.4	96.6	99.8	100.2	97.2	100.3	96.5	95.5	100.1	96.7	99.7	96.9	94.3	100.0	100.3		100.5	97.1	99.4
# oxygen	12	23	8	25	5	12	23	8	25	22	12	23	8	25	22	12	6		8	23	6
Si	3.0	6.4	2.8	6.2	1.0	3.0	6.1	2.8	6.2	5.9	3.0	6.3	2.8	6.1	6.0	3.0	1.9		2.8	6.3	2.0
Ti	0.0	0.1	0.0	0.0	0.0	0.0	0.1	0.0	0.0	0.0	0.0	0.1	0.0	0.0	0.0	0.0	0.0		0.0	0.1	0.0
Al	2.0	2.9	1.2	5.1	2.0	2.0	3.0	1.2	5.1	6.0	2.0	2.9	1.2	5.1	6.0	2.0	0.3		1.2	2.6	0.1
Cr	0.0	0.0	0.0	0.0	0.0	0.0	0.0	0.0	0.0	0.0	0.0	0.0	0.0	0.0	0.0	0.0	0.0		0.0	0.0	0.0
Fe	1.7	1.8	0.0	1.1	0.0	1.8	1.7	0.0	1.0	0.1	1.8	1.9	0.0	1.1	0.1	1.4	0.2		0.0	1.7	0.2
Mn	0.1	0.0	0.0	0.0	0.0	0.1	0.0	0.0	0.0	0.0	0.1	0.0	0.0	0.0	0.0	0.0	0.0		0.0	0.0	0.0
Mg	0.7	1.3	0.0	0.0	0.0	0.6	2.2	0.0	0.0	0.0	0.6	2.2	0.0	0.0	0.0	0.6	0.6		0.0	2.4	0.7
Ca	0.5	1.7	0.2	4.0	0.0	0.6	1.6	0.2	3.9	0.1	0.6	1.6	0.2	4.0	0.1	1.0	0.8		0.2	1.7	0.9
Na	0.0	0.6	0.8	0.0	0.0	0.0	0.8	0.8	0.0	1.7	0.0	0.6	0.8	0.0	1.7	0.0	0.2		0.8	0.8	0.1
K	0.0	0.1	0.0	0.0	0.0	0.0	0.1	0.0	0.0	0.2	0.0	0.1	0.0	0.0	0.2	0.0	0.0		0.0	0.2	0.0
Total	8.0	14.8	5.0	16.3	3.0	8.0	15.7	5.0	16.2	14.0	8.0	15.6	5.0	16.3	14.0	8.0	4.0		5.0	15.8	4.0

$X_{An} = [Ca/(Ca + Na)] = 0.20–0.36$. The coarse-grained plagioclase shown in Fig. 3 is oligoclase and the more andesine compositions are from the films of plagioclase along grain boundaries (arrow 2 in CaO map, Fig. 3). Plagioclase in dioritic gneiss that hosts sites of former partial melting is oligoclase with $X_{An} = 0.17–0.26$. Plagioclase intergrown with kyanite (Fig. 4) is oligoclase with $X_{An} = 0.19–0.23$. S4 plagioclase straddles the oligoclase/andesine boundary with $X_{An} = 0.28–0.32$. Post-S4 plagioclase intergrown with biotite at sites of former phengite breakdown (Figs 5e,f & 6) is andesine to labradorite with $X_{An} = 0.36–0.52$. Coarse-grained and fine-grained plagioclase in sample ARC5C (Fig. 7) is oligoclase to andesine with $X_{An} = 0.14–0.31$.

Paragonite from across the Arthur River Complex has $X_{Na} = [Na/(Na + K)] = 0.79–0.88$ and 2.87–2.98 silica cations per formula unit (p.f.u., 11 oxygen; Fig. 8b). The muscovite substitution in the paragonite is most commonly approximately 15%. Phengite from across the Arthur River Complex has $X_{Na} = [Na/(Na + K)] = 0.10–0.46$ and 3.02–3.28 silica cations p.f.u. (11 oxygens; Fig. 8b). However, most phengite grains have *c.* 3.1 silica cations p.f.u. The paragonite substitution in the phengite is approximately 20%. The small spread in data plotted in Fig. 8(b) is observed both within and between samples. Hornblende across the Arthur River Complex is mostly pargasite with less ferro-pargasite (after Leake *et al.*, 1997); $X_{Mg} = [Mg/(Mg + Fe)]$ is mostly between 0.52 and 0.63. Kyanite generally contains < 1 wt% Fe^{3+}.

THERMOBAROMETRY

P–T estimates obtained from applying a variety of thermobarometric techniques to the mineral assemblages described above are summarised in Table 4. Sample 9802 contains garnet (texturally indistinct from that shown in Fig. 3) in grain contact with kyanite, plagioclase and quartz (texturally indistinct from that

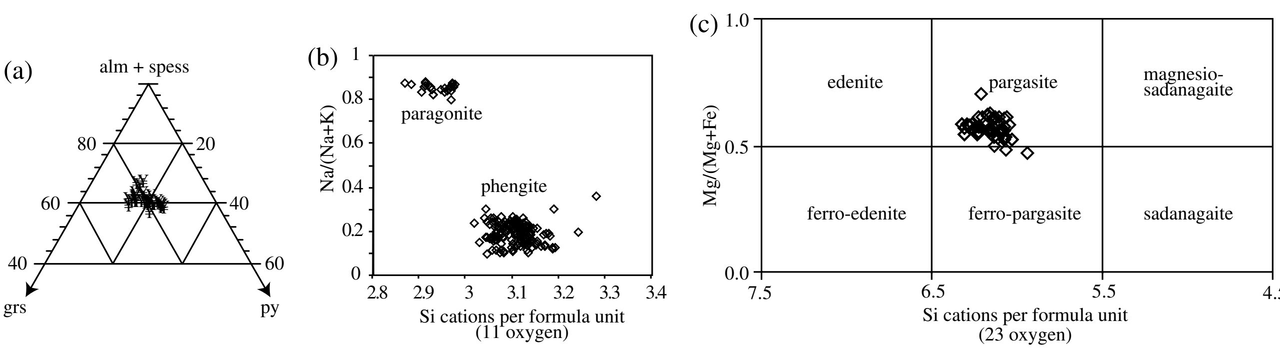

Fig. 8. Representative compositions from the assemblages discussed in the text for (a) garnet (b) white mica and (c) hornblende.

Table 4. *P–T* estimates.

Sample	Location Milford 1 : 50 000 metric grid	Assemblage	Timing	Assumed		Calculated result		Method	
				P (kbar)	*T* (°C)	*T* (°C)	*P* (kbar)	*T*	*P*
9802	Pembroke Ck 21044 56120	Grt-Hbl-Czo-Pl-Qtz-Ky	Cooling	12	650	11.7, 12.2	3	1, 2	
				13.3	677	677 ± 64	13.3 ± 2.2	5	5
9831X	Pembroke Ck 21044 56121	Grt-Hbl-Czo-Pl-Qtz-Ky	Cooling	12	650	11.4, 12.2	3	1, 2	
				12.9	653	653 ± 46	12.9 ± 1.6	5	5
9828	Pembroke Ck 21043 56124	Grt-Hbl-Pg-Pl-Czo-Qtz	Hydration	12	650	703	11.1	3	1
				13.1	687	687 ± 34	13.1 ± 1.4	5	5
PK5	Lake Pukutahi 21086 56164	Grt-Hbl-Pg-Pl-Czo-Qtz	S4	12	650	736	11.4	3	1
				13.2	694	694 ± 42	13.2 ± 1.7	5	5
PK4	Lake Pukutahi 21082 56167	Grt-Hbl-Phengite-Pl-Czo-Qtz	S4	12	650	704	10.9	3	1
				11.9	629	629 ± 56	11.9 ± 1.8	5	5
PK7B	Lake Pukutahi 21071 56163	Grt-Bt-Phengite-Pl-Qtz	Post S4	9	605	4			
				8.8	677	677 ± 52	8.8 ± 1.5	5	5
ARC5C	Mt Daniel 20083 56130	Grt-Cpx-Hbl-Pl-Qtz	Post S4?	14	800	869	14.7	3	1
				14	800	667	14.9	6	7
				14.4	688	688 ± 58	14.4 ± 1.9	5	5

Methods:
1 Kohn & Spear (1990); 2 Newton & Haselton (1981); 3 Graham & Powell (1984); 4 Perchuk & Lavrent'eva (1983); 5 Powell & Holland (1988); 6 Ellis & Green (1979); 7 Newton & Perkins (1982).

shown in Fig. 5a,b). The garnet shows no embayments and is assumed to be in equilibrium with the kyanite intergrowths. Compositions of adjacent grains (Table 4) give pressure estimates of $P = 12.2$ kbar for an estimated $T = 650$ °C (after Newton & Haselton, 1981). In sample 9802, garnet is also in grain contact with hornblende, plagioclase and quartz. The assemblage garnet, hornblende, plagioclase and quartz yield pressure estimates of 11.7 kbar for an estimated $T = 650$ °C (after Kohn & Spear, 1990). *P–T* conditions may also be estimated using the average pressure-temperature approach of THERMOCALC (v.2.6; Powell & Holland, 1988), with the internally consistent thermodynamic data set of Holland & Powell (1990; data file created April 1996). All mineral end-member activities were calculated using the computer program AX (Holland, 1993) and the defaults suggested in Powell & Holland (1988). All results quoted from THERMOCALC below show 2σ errors. Using the average *P* approach of THERMOCALC, the assemblage garnet, hornblende, clinozoisite, plagioclase, kyanite and quartz in samples 9802 and 9831X (which contains identical textures to those described for 9802) give 13.3 ± 2.2 kbar and 12.9 ± 1.6 kbar, respectively, which are within error of the directly calibrated barometric results (Table 4). Using the average *T* approach of THERMOCALC, the same assemblage in samples 9802 and 9831X give 677 ± 64 °C and 653 ± 46 °C, respectively (Table 4).

Gabbroic gneiss (sample 9828) from the Pembroke Granulite also contains paragonite-bearing assemblages. The compositions of adjacent grains of garnet, hornblende, plagioclase and quartz in sample 9828 give pressure estimates of 11.1 kbar for an estimated $T = 650$ °C (after Kohn & Spear, 1990). The same sample and assemblage give temperature estimates of 703 °C for an estimated $P = 12$ kbar (after Graham & Powell, 1984). Using the average *P* and average *T* approach of THERMOCALC, the assemblage garnet, hornblende, clinozoisite, plagioclase, paragonite and quartz in sample 9828 gives 13.1 ± 1.4 kbar and 687 ± 34 °C, which are within error of the directly calibrated thermobarometric results (Table 4).

Milford Gneiss samples PK4 and PK5 contain well-developed phengite and paragonite-bearing S4 mineral assemblages. All minerals used in thermobarometric calculations were in grain contact and show no reaction between grains. The compositions of adjacent grains of S4 garnet, hornblende, plagioclase and quartz in sample PK5 give pressure estimates of 11.4 kbar for an estimated 650 °C (after Kohn & Spear, 1990). The same sample and assemblage gives temperature estimates of 736 °C for an estimated $P = 12$ kbar (after Graham & Powell, 1984). Using the average *P* and average *T* approach of THERMOCALC, the assemblage garnet, hornblende, clinozoisite, plagioclase, paragonite and quartz in sample PK5 gives 13.2 ± 1.7 kbar and 694 ± 42 °C, which are within error of the directly calibrated thermobarometric results (Table 4).

For Milford Gneiss sample PK4, the compositions of adjacent grains of garnet, hornblende, plagioclase and quartz give pressure estimates of 10.9 kbar for an estimated 650 °C (after Kohn & Spear, 1990). The same sample and assemblage gives temperature estimates of 704 °C for an estimated 12 kbar (after Graham & Powell, 1984). Using the average *P* and average *T* approach of THERMOCALC, the assemblage garnet, hornblende, clinozoisite, plagioclase, phengite and quartz in sample PK4 gives 11.9 ± 1.8 kbar and 629 ± 56 °C, which is a slightly lower temperature estimate than that obtained from the directly calibrated thermometry (Table 4).

For the selvage around the post-D4 pegmatite (sample PK7B, Fig. 5d), the compositions of adjacent grains of garnet and biotite give temperature estimates of 605 °C for an estimated $P = 9$ kbar (after Perchuk & Lavrent'eva, 1983). Using the average *P* and average

T approach of THERMOCALC, the assemblage garnet, biotite, phengite, plagioclase and quartz in sample PK7B gives $P = 8.8 \pm 1.5$ kbar and $T = 677 \pm 52$ °C, which is slightly higher temperature than the directly calibrated thermometry results (Table 4).

Sample ARC5C from the contact aureole of the Western Fiordland Orthogneiss at Mt Daniel contains the peak assemblage garnet, jadeitic diopside, hornblende, plagioclase and quartz (Fig. 7). Core analyses of coarse-grained unzoned minerals were used in the thermobarometric calculations. The compositions of adjacent grains of garnet, jadeitic diopside, plagioclase and quartz give pressure estimates of 14.9 kbar for an estimated $T = 800$ °C (after Newton & Perkins, 1982). The same sample and assemblage gives temperature estimates of 855 °C for an estimated $P = 14$ kbar (after Ellis & Green, 1979). If a correction is made for Fe^{3+} in clinopyroxene, then the temperature estimates drop to 667 °C (Table 4). The compositions of adjacent grains of garnet, hornblende, plagioclase and quartz give pressure estimates of 14.7 kbar for an estimated $T = 800$ °C (after Kohn & Spear, 1990). The same sample and assemblage gives temperature estimates of 869 °C for an estimated $P = 14$ kbar (after Graham & Powell, 1984). Using the average *P* and average *T* approach of THERMOCALC, the assemblage garnet, jadeitic diopside, hornblende, plagioclase and quartz in sample ARC5C gives 14.4 ± 1.9 kbar and 688 ± 48 °C, which is a slightly lower temperature estimate than that obtained from the directly calibrated thermometry (Table 4).

P–T and *T–*M_{H_2O} pseudosections

The thermobarometric results indicate that the kyanite, paragonite and phengite-bearing assemblages evolved in the deep crust ($P = 11–13$ kbar) at temperatures of *c.* 600–700 °C. The petrological analysis of the paragonite and phengite-bearing assemblages presented above suggests that water played a vital role in the development of the white mica-bearing assemblages. However, the available thermobarometric techniques give no information with respect to the proportion of fluid that accompanied the development of the kyanite and paragonite (with or without phengite) bearing assemblages. *P–T* pseudosections, calculated with H_2O in excess, are suitable where H_2O-saturated conditions can be inferred, but inappropriate for examining mineralogical changes that involved H_2O-undersaturated conditions, as for example inferred for the development of the kyanite-bearing intergrowth textures.

To examine the changes in conditions associated with the kyanite and paragonite textures only, quantitative *P–T* and $T–M_{H_2O}$ pseudosections (Guiraud *et al.*, 2001) have been constructed in the model system CNFMASH (CaO-Na_2O-FeO-MgO-Al_2O_3-SiO_2-H_2O), using THERMOCALC (version 2.75) and the '20 April 1996' internally consistent thermodynamic data set (Powell *et al.*, 1998). Details of the use of THERMOCALC for grid and pseudosection construction are outlined in Powell *et al.* (1998). Minerals included in the construction of the grid are garnet (Grt), hornblende (Hbl), paragonite (Pg), clinozoisite (Czo), kyanite (Ky), orthopyroxene (Opx), clinopyroxene (Cpx), plagioclase (Pl) and quartz (Qtz). Most of the activity models used in the calculations assume ideal mixing on all sites and are identical to those used by Powell *et al.* (1998). The modelled rock composition was obtained from bulk rock analysis of element maps of oxide weight percent for sample 9805. The bulk rock composition is calculated from the element maps by averaging the composition of the whole area mapped (see Clarke *et al.*, 2001; Marmo *et al.*, 2002). This technique is useful when trying to model textures within a particular compositional domain from heterogeneous rocks. In this case the bulk rock calculated for sample 9805 from element maps is similar to XRF whole rock analyses from other dioritic gneiss samples of the Pembroke Granulite (Table 3 in Daczko *et al.*, 2001b) and suggests that the compositional domain modelled for in this paper approximates the whole rock. Where present, the fluid phase is assumed to be pure H_2O. In the $T–M_{H_2O}$ diagram H_2O is considered explicitly (Guiraud *et al.*, 1996; Carson *et al.*, 1999; Clarke *et al.*, 2000): M_{H_2O} is defined as the molar proportion of the component, H_2O, in the bulk composition. We define a bulk rock with 0 wt % H_2O and 100 wt % ($CaO + Na_2O + FeO + MgO + Al_2O_3$) as $M_{H_2O} = 0$ and a bulk rock with 50 wt % H_2O and 50 wt % ($CaO + Na_2O + FeO + MgO + Al_2O_3$) as $M_{H_2O} = 1$. Therefore, for example, a bulk rock with 20 wt % H_2O has $M_{H_2O} = 0.4$ by definition.

Figure 9 represents *P–T* and $T–M_{H_2O}$ pseudosections appropriate to the bulk composition of the dioritic gneiss of the Pembroke Granulite. On two-dimensional diagrams such as these, one variable (*P*, *T* or M_{H_2O}) must be held constant. As a starting point, *P* and *T* were modelled by holding M_{H_2O} constant at water saturated conditions (Fig. 9a). Although it is unlikely that these rocks were ever water saturated, Fig. 9(a) indicates that kyanite is not stable at the water saturated *P–T* conditions modelled and paragonite is only stable at $P > 8$ kbar and $T < c.$ 650 °C. Figure 9(a) also shows: (i) the *P–T* conditions inferred to have accompanied partial melting (pre-D4, dark grey box; Clarke *et al.*, 2000; Daczko *et al.*, 2001b); (ii) thermobarometric results for S4 and paragonite-kyanite-bearing assemblages calculated using THERMOCALC and presented above (error ellipses shaded light grey); and (iii) thermobarometric results for assemblages in the Anita Shear Zone (Klepeis *et al.*, 1999) that cut S4 (error ellipse shaded medium grey). The effect of cooling at H_2O-undersaturated conditions can be illustrated on a 2D diagram by fixing pressure. On the basis of the thermobarometric constraints presented in Fig. 9(a) and those outlined above for the kyanite and paragonite textures, the $T–M_{H_2O}$ diagram (Fig. 9b)

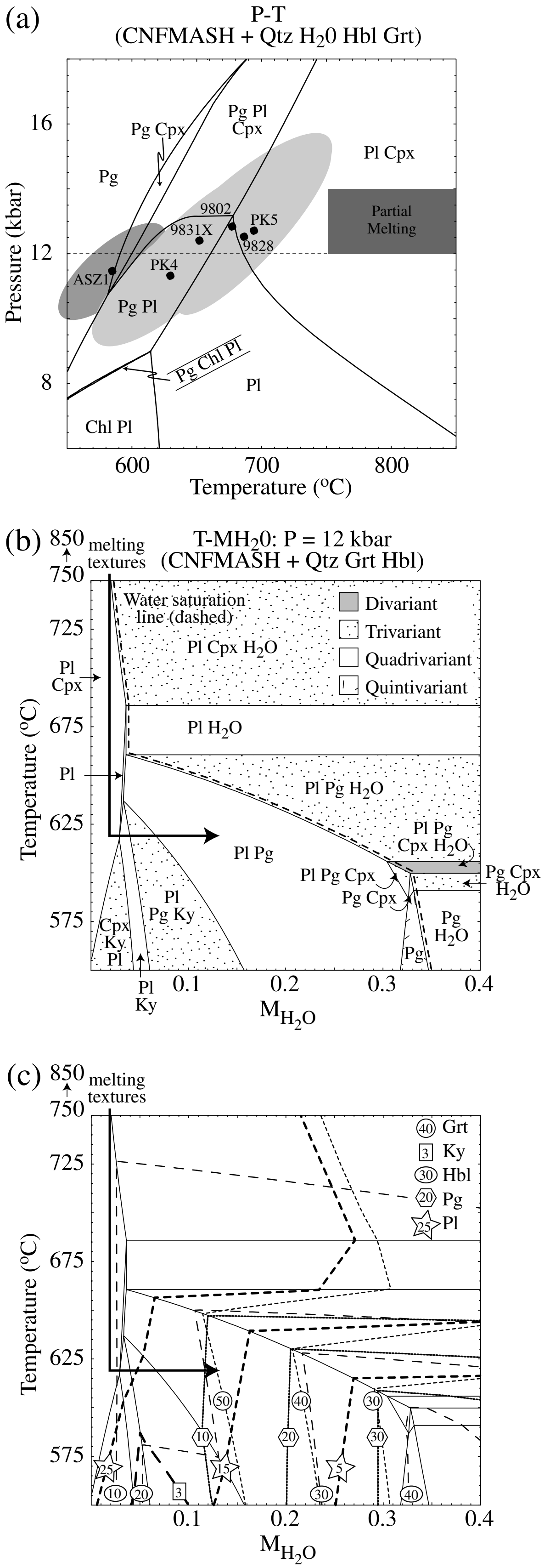

is drawn for $P = 12$ kbar and $T = 550$–750 °C (dashed line on Fig. 9a). The modelled rock composition, on a molar basis, varies with water content (Fig. 9b) from CaO = 17.70, Na_2O = 9.10, FeO = 28.90, MgO = 14.55, Al_2O_3 = 29.74, H_2O = 0.00 ($M_{H_2O} = 0$) to CaO = 14.16, Na_2O = 7.28, FeO = 23.12, MgO = 11.64, Al_2O_3 = 23.79, H_2O = 20 ($M_{H_2O} = 0.4$). The pseudosection was also calculated with quartz in excess, and illustrates the mineral evolution with respect to changing temperature and M_{H_2O}, as well as the preservation of various mineral assemblages in terms of recrystallization and fluid availability. A horizontal line on the diagram represents the addition or subtraction of H_2O at any given temperature. The indicated H_2O-saturation line is the limiting boundary beyond which any further increase of M_{H_2O} mainly increases the mode of fluid. Figure 9(b) illustrates the dependence of the modelled assemblages on T and M_{H_2O}. Garnet (Grt) and hornblende (Hbl) are stable in every field on the diagram and are therefore not labelled in each field but at the top of the figure along with the excess phase quartz (Qtz). Clinopyroxene is stable at $T > 685$ °C and $M_{H_2O} < c.\ 0.04$, however, the mode of clinopyroxene is mostly much $\ll 5\%$, suggesting that it does not play a vital role in the assemblage changes predicted by the model.

Fig. 9. (a) P–T pseudosection for $P = 6$–18 kbar and $T = 550$–850 °C, constructed in the model system CNFMASH (CaO-Na_2O-FeO-MgO-Al_2O_3-SiO_2-H_2O), using THERMOCALC (version 2.75) and the '20 April 1996' internally consistent thermodynamic data set (Powell *et al.*, 1998). The bulk rock composition used to construct the diagram is CaO = 17.70, Na_2O = 9.10, FeO = 28.90, MgO = 14.55, Al_2O_3 = 29.74, quartz and water in excess. Minerals included in the construction of the grid are garnet (Grt), hornblende (Hbl), paragonite (Pg), clinozoisite (Czo), kyanite (Ky), orthopyroxene (Opx), clinopyroxene (Cpx), and plagioclase (Pl). Divariant fields are labelled with three phases; trivariant fields are labelled with two phases and quadrivariant fields are labelled with one phase. Garnet and hornblende are stable across the entire diagram. The dashed line at $P = 12$ kbar is where Fig. 9 (b) projects into the page away from water saturated conditions, along the M_{H_2O} (molar proportion of water) axis. The dark grey box represents metamorphic conditions that accompanied partial melting of these rocks (Clarke *et al.*, 2000; Daczko *et al.*, 2001b); it indicates peak P–T conditions for northern Fiordland. The black dots are thermobarometry results for the S4 and paragonite-kyanite-bearing assemblages presented in Table 4 (THERMOCALC, error ellipses shaded grey). The medium grey error ellipse surrounds data for P–T conditions that accompanied Anita Shear Zone 1 (Klepeis *et al.*, 1999); ASZ1 cuts S4 and provides a lower limit to the P–T conditions and textures modelled in this paper. (b) T–M_{H_2O} pseudosection for $P = 12$ kbar and $T = 550$–750 °C. The bulk rock composition ranges from CaO = 17.70, Na_2O = 9.10, FeO = 28.90, MgO = 14.55, Al_2O_3 = 29.74, H_2O = 0.00 ($M_{H_2O} = 0$) to CaO = 14.16, Na_2O = 7.28, FeO = 23.12, MgO = 11.64, Al_2O_3 = 23.79, H_2O = 20 ($M_{H_2O} = 0.4$). The fluid phase is assumed to be pure H_2O. M_{H_2O} is defined as the molar proportion of the component, H_2O, in the bulk composition (Guiraud *et al.*, 2001). A horizontal line on the diagram represents the addition or subtraction of H_2O at a given temperature. Garnet and hornblende are stable across the entire diagram. (c) Fig. 9(b) contoured for mineral modes.

Changes in mineralogy of the northern Fiordland rocks involved, in summary: (1) the consumption of hornblende, with or without clinozoisite, plagioclase and quartz, during melting; (2) the consumption of plagioclase, with or without hornblende and quartz, to form intergrowths of kyanite, quartz and plagioclase; (3) the consumption of kyanite, plagioclase and garnet to form paragonite and phengite. As the model does not account for the presence of any melt phase, the diagram does not help in understanding the partial melting textures or conditions at which partial melting occurred. However, the position of the melting textures must lie below the water saturation line and at temperatures greater than 750 °C (Daczko *et al.*, 2001b). These partial melting conditions lie above the top of Fig. 9(b), but provide a probable starting position for the inferred T–M_{H_2O} path. The modelling suggests that kyanite (Ky) would become stable if the rock cooled below 635 °C at $P = 12$ kbar. The thermobarometry outlined above suggests that the kyanite-bearing textures in samples 9802 and 9831X developed at pressures of approximately 12 kbar and temperatures of 605–740 °C, taking into account the 2 σ errors on the temperature estimates. The high temperatures indicated by the thermobarometry may reflect a mixed population of grains, involving some that grew during the high-T metamorphic conditions. On the basis of conditions indicated for kyanite-bearing assemblages in the pseudosection, we prefer the lower temperature end of the range of thermometry results.

The development of the phengite-bearing assemblages is not modelled; we have not included K in the model system as phengite would be the only potassic mineral. As phengite occurs with paragonite, it is inferred that it will broadly follow the same trends as paragonite in the model. The introduction of paragonite and phengite as stable phases in the rocks must have involved the addition of H_2O to the rocks and can be represented by a horizontal line on the pseudosection. The small modes of paragonite and phengite in samples 9828, PK4 and PK5 (generally < 10%) are consistent with $T = 575$–625 °C and $M_{H_2O} \approx 0.12$ (Fig. 9). Such conditions involve slightly lower temperatures than the thermobarometry presented above (by < 50 °C).

Critical textural evidence in the rocks involves: (1) plagioclase in leucosomes and S1 plagioclase, with or without hornblende, being partially pseudomorphed by intergrowths of kyanite, quartz and plagioclase; (2) kyanite being cut by paragonite; and (3) paragonite, with or without phengite and hornblende, partially pseudomorphing garnet during hydration related to the development of S4. A T–M_{H_2O} path that can account for these features is indicated by an arrow on Fig. 9(b); the terrane would need to cool by at least 100 °C and by up to 200 °C from peak conditions to reach kyanite-bearing fields. The progressive addition of small proportions of water would have taken the rocks through the kyanite-bearing field, into the kyanite-paragonite-bearing field and finally out of the kyanite-bearing fields into a garnet-hornblende-paragonite-plagioclase quadrivariant field. Along such a path, kyanite would have been introduced and then consumed, garnet and plagioclase modes would have decreased by *c.* 10% each, and hornblende and paragonite modes increased by *c.* 10% each. The modelling does not take into account Fe^{3+} or Ti contents in any mineral. Fe^{3+} is likely to have had stabilised clinozoisite – it occurs in all samples – but is not stable anywhere in the model system.

DISCUSSION

Paragonite-hornblende-bearing assemblages in mafic rocks are indicators of high-P regional metamorphism (Konzett & Hoinkes, 1996). Hornblende-bearing mafic rocks of the Arthur River Complex in northern Fiordland, New Zealand were buried to depths in excess of 45 km during the Early Cretaceous and experienced temperatures sufficiently elevated to promote incongruent partial melting in dioritic lithologies (Clarke *et al.*, 2000; Daczko *et al.*, 2001b; Fig. 10(a)). The simultaneous development of garnet-clinopyroxene

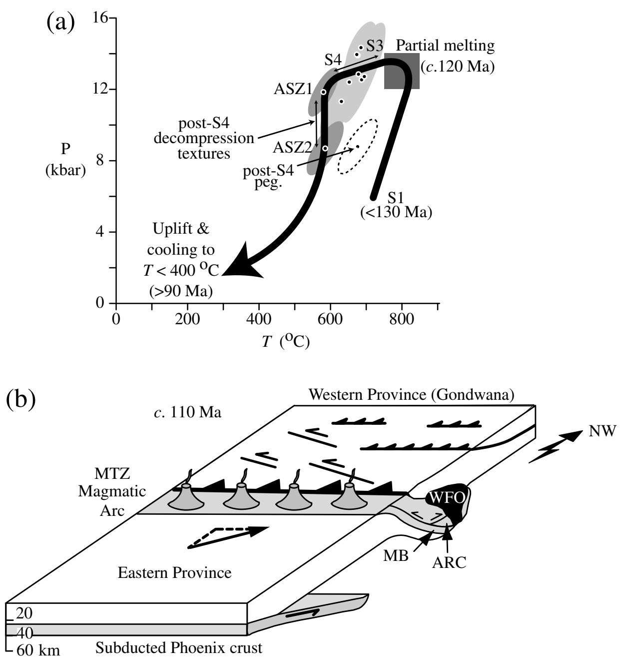

Fig. 10. (a) Anticlockwise P–T path for the Arthur River Complex. Points on the path are compiled from Clarke *et al.* (2000) for S1 and D2 (grey box), Daczko *et al.* (2001a) for S3, thermobarometric results in this paper for S4, Klepeis *et al.* (1999) for Anita Shear Zone 1 and 2 (ASZ1, ASZ2). Shaded ellipses are THERMOCALC error ellipses. The geochronologic constraints are from data presented in Table 2. (b) Tectonic cartoon constructed for *c.* 110 Ma showing an obliquely convergent arc-continent collisional setting (modified from Daczko *et al.*, 2001a). Eastern and Western Provinces are shown. MB = Median Batholith; ARC = Arthur River Complex; WFO = Western Fiordland Orthogneiss. Note the tectonic burial and under thrusting of the leading edge of the Median Batholith beneath the Arthur River Complex.

reaction zones in gabbroic rocks of the Pembroke Granulite, with the partial melting of dioritic rocks (Daczko *et al.*, 2001b), suggests that temperatures accompanying partial melting were between 750–850 °C (table 2 in Clarke *et al.*, 2000). S1 assemblages and leucosome that encloses peritectic garnet were overgrown by random intergrowths of kyanite, quartz and plagioclase. The mineral chemistry of these assemblages indicate that metamorphic conditions of $P = 11–13$ kbar and $T = 600–700$ °C accompanied the development of the intergrowths. The results of thermobarometry and consideration of $P–T$ and $T–M_{H_2O}$ modelling at fixed $P = 12$ kbar suggest that the kyanite intergrowths developed in response to cooling of the rocks, at depth, by 100–200 °C with minor change in pressure (Fig. 10a). Paragonite and phengite-bearing assemblages that partially to completely pseudomorph kyanite and garnet, also formed at metamorphic conditions of $P = 11–13$ kbar and $T = 600–700$ °C. The micaceous assemblages represent appreciable hydration of the rocks at some point on their cooling path (e.g. Barnicoat & Fry, 1986). Our $P–T$ estimates for the Fiordland rocks are similar to those inferred for paragonite-hornblende-bearing assemblages from the Austroalpine Schneeberg Complex in southern Tyrol, Italy (Konzett & Hoinkes, 1996). They corroborate conclusions reached by Evans (1990) and Konzett & Hoinkes (1996), that paragonite and calcic hornblende assemblages reflect restricted $P–T$ conditions within the epidote-amphibolite facies for mafic rocks. The thermobarometric results indicate that the high-P conditions prevailed during cooling of the Fiordland block; rapid exhumation cannot be invoked as the cause of the changes in mineral assemblage, in contrast with models commonly inferred for the cooling of arc rocks. As these large changes in $P–T$ occurred in < 20 Myr, it is unlikely that thermal relaxation of the deep crust led to the rapid cooling.

As part of the final stage of metamorphism in the rocks described in this study, phengite was partially replaced by biotite and plagioclase, with or without quartz and K-feldspar. The breakdown of phengite and a mafic phase (clinopyroxene, garnet or hornblende) to form biotite and plagioclase is a reaction commonly ascribed to decompression in many lithologies (Lappin & Smith, 1978; Heinrich, 1982; Franz & Spear, 1983; Gomez-Pugnaire *et al.*, 1985; Franz *et al.*, 1986; Konzett & Hoinkes, 1996; Konopásek, 1998). We infer that rapid decompression followed the high-P amphibolite facies conditions, postdating D4 cooling (Fig. 10a). The breakdown of jadeitic diopside to form diopside and plagioclase in samples from Mt Daniel is also a reaction commonly ascribed to decompression (e.g. Elveold & Gilotti, 2000), matching the phengite breakdown textures. The emplacement of the post-D4 pegmatite at $P \approx 9$ kbar also supports an interpretation of decompression following D4 cooling.

The Anita Shear Zone cuts S4 at the western boundary of the Arthur River Complex (Klepeis *et al.*, 1999). Structural and metamorphic data presented by Klepeis *et al.* (1999) suggest that the fabrics of the Anita Shear Zone preserve a record of Cretaceous-Tertiary decompression from $P \approx 12$ kbar and $T \approx 600$ °C (ASZ1 on Fig. 10a) to $P \approx 8.5$ kbar and $T \approx 600$ °C (ASZ2 on Fig. 10a). This decompression is consistent with the phengite breakdown textures presented here, though their timing is uncertain. On the basis of metamorphic conditions estimated for the post-D4 pegmatite, the initial phases of deformation in the Anita Shear Zone (ASZ1) most probably predated the emplacement of the pegmatite. Furthermore, the development of the decompression textures most likely postdates ASZ1, as ASZ1 evolved at high-P (12 kbar). Finally, reactivation of the Anita Shear Zone (ASZ2) during dextral transpression occurred at mid-crustal levels, suggesting that the post-D4 pegmatites were most probably synchronous with or post dated this phase of deformation. The metamorphic data combine in the simplest way to form an anticlockwise $P–T$ path (Fig. 10a). However, we cannot exclude the possibility of heating of the over thickened crust (as would be expected) to produce a small clockwise $P–T$ loop at high-P that would then be followed by near isobaric cooling during D4.

U-Pb zircon ion probe analyses distinguish a Cretaceous metamorphic peak with an average age of *c.* 120 Ma in the Arthur River Complex (Tulloch *et al.*, 2000). K-Ar isotopic dating of hornblende gives ages of *c.* 111–90 Ma (Table 2, Nathan *et al.*, 2000). The apatite cooling ages for the Western Fiordland Orthogneiss, in northern Fiordland, also suggest cooling of the terrane to < 300–400 °C by *c.* 90 Ma (Table 2, Mattinson *et al.*, 1986). The available geochronological data and metamorphic data presented here suggest that the Arthur River Complex cooled rapidly between *c.* 120 and *c.* 90 Ma. Cooling during rapid exhumation is ruled out, on the basis of the persistence of high-P conditions, at least during the early stages of cooling. We propose the following tectonic scenario that involves juxtaposition of the high-T arc rocks with cold crust of the Median Batholith to account for the rapid cooling:

(1) On the basis of U-Pb zircon and apatite ages, and K-Ar hornblende ages, the Darran Complex (major component of Median Batholith in northern Fiordland) was emplaced in the Late Jurassic, at upper crustal conditions ($P < 3$ kbar) and cooled rapidly (Mattinson *et al.*, 1986; Wandres *et al.*, 1998). The Western Fiordland Orthogneiss was emplaced between 126 and 119 Ma, into rocks including the Arthur River Complex, that were at middle to lower crustal conditions ($P < 8$ kbar; Clarke *et al.*, 2000).

(2) Early Cretaceous convergence during arc accretion or collision of the Median Batholith with the palaeo-Pacific margin of Gondwana led to the rapid burial of the Arthur River Complex and Western

Fiordland Orthogneiss to P ≈ 14 kbar (Bradshaw, 1989b; Clarke *et al.*, 2000; Daczko *et al.*, 2001a).

(3) Continued convergence resulted in sinistral pure-shear-dominated shear zones (D3) and deep crustal ductile thrust faults ($P = 14$ kbar) in the Pembroke Granulite (Daczko *et al.*, 2001a). Strain resulting from convergence was partitioned mostly into the Milford Gneiss, producing a well-developed foliation (S4) that evolved during cooling at the root of the magmatic arc.

(4) Cold upper crustal components of the Median Batholith were tectonically buried and juxtaposed against the Arthur River Complex during the waning stages of Early Cretaceous orogenesis. The juxtaposition of the cold crust with the hot rocks led to rapid cooling of the Arthur River Complex and concurrent heating of the leading edge of the Median Batholith.

Metamorphic textures in the Median Batholith at the margin with the Arthur River Complex at Selwyn Creek involve igneous muscovite rimmed by phengite and paragonite, and garnet poikiloblasts enveloped by leucosome (Dockrill, 2000). These textures are consistent with rapid burial and heating of the leading edge of the Median Batholith during convergence (Dockrill, 2000). Dockrill (2000) presents thermobarometric data that suggests the peak metamorphic conditions attained by parts of the Median Batholith adjacent to the Arthur River Complex (at Selwyn Creek) involved $T = 560$–615 °C and $P = 11$–12 kbar. The metamorphic textures and thermobarometry presented by Dockrill (2000) are consistent with our model of rapid cooling in the Arthur River Complex in that they represent an equal and opposite temperature path to that presented here for rocks of the Arthur River Complex. Also, phengite in the Median Batholith displays similar textures to that in the Arthur River Complex suggesting that the Selwyn Creek gneisses of the Median Batholith and Arthur River Complex experienced the same decompression history. Our interpretations are consistent with those of Muir *et al.* (1998), who used geochemical and geochronological data to argue that a Mesozoic magmatic arc, chemically equivalent to the Darran Suite of the Median Batholith, was thrust beneath western Fiordland to depths in excess of 40 km in the Early Cretaceous. This model is also consistent with studies of rocks from elsewhere that conclude that significant parts of the lower crust may be formed from metastably persisting low-*P* assemblages such as those observed throughout most of the Median Batholith (Austrheim & Griffin, 1985; Jamveit *et al.*, 1990; Ellis & Maboko, 1992; White & Clarke, 1997).

CONCLUSIONS

The Arthur River Complex in northern Fiordland, New Zealand was exhumed from the root of a Cretaceous magmatic arc. High-*P* granulite facies conditions, at the root of the arc, formed in a convergent margin setting, and led to the partial melting of dioritic gneiss in the Pembroke Granulite and elsewhere in the Arthur River Complex. Intergrowths of kyanite, quartz and plagioclase and assemblages involving paragonite, with or without phengitic white mica, partially pseudomorph peak metamorphic assemblages. The kyanite-paragonite-phengite-bearing assemblages reflect unusual, short-lived high-*P* cooling of the rocks by up to 200 °C. The rapid cooling of the root of the arc must have occurred in < 20 Myr, and is inferred to have been in response to juxtaposition of the Arthur River Complex with cold upper crustal components of the Median Batholith during convergence (Fig. 10b). Subsequent biotite-plagioclase intergrowths that partially pseudomorph phengite, and diopside-plagioclase intergrowth that partially pseudomorph jadeitic diopside, reflect the postcooling exhumation of the high-*P* terrane.

ACKNOWLEDGEMENTS

Funding to support this work was provided by Australian Research Council funding to KAK and GLC (grant number A10009053) and National Science Foundation funding to KAK (EAR-0087323). An Australian Postgraduate Award supported NRD. We thank N. Mortimer and A. Tulloch of the IGNS, Dunedin for many helpful discussions and logistical assistance, and the Department of Land Conservation in Te Anau for permission to visit and sample localities in the Fiordland National Park. Thanks go to R. L. Turner, J. A. Stevenson and A. Papadakis for their enthusiastic assistance in the field. Critical reviews by S. L. Harley and D. L. Whitney, and careful editorial work by R. Powell improved an earlier version of this manuscript.

REFERENCES

Austrheim, H. & Griffin, W. L., 1985. Shear deformation and eclogite formation within granulite-facies anorthosites of the Bergen Arcs, western Norway. *Chemical Geology*, **50,** 267–281.

Barnicoat, A. C. & Fry, N., 1986. High-pressure metamorphism of the Zermatt-Saas ophiolite zone, Switzerland. *Journal of the Geological Society of London*, **143,** 607–618.

Bence, A. E. & Albee, A. L., 1968. Empirical correction factors for the electron microanalysis of silicates and oxides. *Journal of Geology*, **76,** 382–403.

Bishop, D. G., Bradshaw, J. D. & Landis, C. A., 1985. Provisional terrain map of South Island, New Zealand. In: *Tectonostratigraphic Terranes of the Circum-Pacific Region* (eds Howell, D. G., Jones, D. L., Cox, A. & Nur, A.), pp. 512–522. Circum-Pacific Council for Energy and Resources, Houston.

Blattner, P., 1976. Replacement of hornblende by garnet in granulite facies assemblages near Milford Sound, New Zealand. *Contributions to Mineralogy and Petrology*, **55,** 181–190.

Blattner, P., 1978. Geology of the crystalline basement between Milford Sound and the Hollyford Valley, New Zealand. *New Zealand Journal of Geology and Geophysics*, **21,** 33–47.

Blattner, P., 1991. The North Fiordland transcurrent convergence. *New Zealand Journal of Geology and Geophysics*, **34,** 542–553.

Bradshaw, J. Y., 1989a. Origin and metamorphic history of an Early Cretaceous polybaric granulite terrain, Fiordland, southwest New Zealand. *Contributions to Mineralogy and Petrology*, **103,** 346–360.

Bradshaw, J. Y., 1989b. Early Cretaceous vein-related garnet granulite in Fiordland, southwest New Zealand: a case for infiltration of mantle-derived CO_2-rich fluids. *Journal of Geology*, **97,** 697–717.

Bradshaw, J. Y., 1990. Geology of crystalline rocks of northern Fiordland: details of the granulite facies Western Fiordland Orthogneiss and associated rock units. *New Zealand Journal of Geology and Geophysics*, **33,** 465–484.

Carson, C. J., Powell, R. & Clarke, G. L., 1999. Calculated mineral equilibria for the eclogite facies in Na_2O-CaO-FeO-MgO-Al_2O_3-SiO_2-H_2O: application to the Pouébo Terrane, Pam Peninsula, New Caledonia. *Journal of Metamorphic Geology*, **17,** 9–24.

Clarke, G. L., Daczko, N. R. & Nockolds, C., 2001. A method for applying matrix corrections to X-ray intensity maps using the Bence-Albee algorithm and Matlab. *Journal of Metamorphic Geology*, **19,** 635–644.

Clarke, G. L., Klepeis, K. A. & Daczko, N. R., 2000. Cretaceous high-P granulites at Milford Sound, New Zealand: their metamorphic history and emplacement in a convergent margin setting. *Journal of Metamorphic Geology*, **18,** 359–374.

Daczko, N. R., Clarke, G. L. & Klepeis, K. A., 2001b. Transformation of two-pyroxene hornblende granulite to garnet granulite involving simultaneous melting and fracturing of the lower crust, Fiordland, New Zealand. *Journal of Metamorphic Geology*, **19,** 547–560.

Daczko, N. R., Klepeis, K. A. & Clarke, G. L., 2001a. Evidence of Early Cretaceous collisional-style orogenesis in northern Fiordland, New Zealand and its effects on the evolution of the lower crust. *Journal of Structural Geology*, **23,** 693–713.

Daczko, N. R., Stevenson, J. A., Clarke, G. L. & Klepeis, K. A., 2003. Successive hydration and dehydration of a high-*P* mafic hornfels involving clinopyroxene-kyanite symplectites, Mt Daniel, Fiordland, New Zealand. *Journal of Metamorphic Geology*, in press.

Dockrill, B. R., 2000. The Decompressional History of Northern Fiordland and its Relationship to a Cretaceous-Tertiary Crustal Scale Shear Zone. Unpublished *BSc (Honours) Thesis*, *University of Sydney, Sydney*.

Ellis, D. J. & Green, D. H., 1979. An experimental study of the effect of Ca upon garnet-clinopyroxene Fe-Mg exchange equilibria. *Contributions to Mineralogy and Petrology*, **71,** 13–22.

Ellis, D. J. & Maboko, M. A. H., 1992. Precambrian tectonics and the physiochemical evolution of the continental crust. I. The gabbro-eclogite transition revisited. *Precambrian Research*, **55,** 491–506.

Elveold, S. & Gilotti, J. A., 2000. Pressure-temperature evolution of retrogressed kyanite eclogites, Weinschenk Island, North-East Greenland Caledonides. *Lithos*, **53,** 127–147.

Evans, B. W., 1990. Phase relations of epidote-blueschists. *Lithos*, **25,** 3–23.

Franz, G. & Spear, F. S., 1983. High pressure metamorphism of siliceous dolomites from the Central Tauern Window, Austria. *American Journal of Science*, **283,** 396–413.

Franz, G., Thomas, S. & Smith, D. C., 1986. High-pressure phengite decomposition in the Weissenstein eclogite, Munchberger Gneiss Massif, Germany. *Contributions to Mineralogy and Petrology*, **92,** 71–85.

Gibson, G. M., McDougall, I. & Ireland, T. R., 1988. Age constraints on metamorphism and the development of a metamorphic core complex in Fiordland, southern New Zealand. *Geology*, **16,** 405–408.

Gomez-Pugnaire, M. T., Visona, D. & Franz, G., 1985. Kyanite, margarite and paragonite in pseudomorphs in amphibolitized eclogites from the Betic Cordilleras, Spain. *Chemical Geology*, **50,** 129–141.

Graham, C. M. & Powell, R., 1984. A garnet-hornblende geothermometer; calibration, testing, and application to the Pelona Schist, Southern California. *Journal of Metamorphic Geology*, **2,** 13–31.

Guiraud, M., Powell, R. & Cottin, J.-Y., 1996. Hydration of orthopyroxene-cordierite-bearing assemblages at Laouni, Central Hoggar, Algeria. *Journal of Metamorphic Geology*, **14,** 467–476.

Guiraud, M., Powell, R. & Rebay, G., 2001. H_2O in metamorphism and unexpected behaviour in the preservation of metamorphic mineral assemblages. *Journal of Metamorphic Geology*, **19,** 445–454.

Heinrich, ChA., 1982. Kyanite-eclogite to amphibolite facies evolution of hydrous mafic and pelitic rocks, Adula Nappe, Central Alps. *Contributions to Mineralogy and Petrology*, **81,** 30–38.

Hill, E. J., 1995a. The Anita Shear Zone: a major, middle Cretaceous tectonic boundary in northwestern Fiordland. *New Zealand Journal of Geology and Geophysics*, **38,** 93–103.

Hill, E. J., 1995b. A deep crustal shear zone exposed in western Fiordland, New Zealand. *Tectonics*, **14,** 1172–1181.

Holland, T. J. B., 1993. Computer program AX. http://www.esc.cam.ac.uk/new/v10/links/software.html.

Holland, T. J. B. & Powell, R., 1990. An enlarged and updated internally consistent dataset with uncertainties and correlations: the system K_2O-Na_2O-CaO-MgO-MnO-FeO-Fe_2O_3-Al_2O_3-TiO_2-SiO_2-C-H_2-O_2. *Journal of Metamorphic Geology*, **8,** 89–124.

Jamveit, B., Bucher-Nurminen, K. & Austrheim, H., 1990. Fluid controlled eclogitization of granulites in deep crustal shear zones, Bergen Arcs, western Norway. *Contributions to Mineralogy and Petrology*, **104,** 184–193.

Johannes, W. & Holtz, F., 1991. Formation and composition of H_2O-undersaturated granitic melts. In: *High Temperature Metamorphism and Crustal Anatexis, Mineralogical Society Special Publications* (eds Ashworth, J. R. & Brown, M.), pp. 87–104. Unwin-Hyman, London.

Kimbrough, D. L., Tulloch, A. J., Coombs, D. S., Landis, C. A., Johnston, M. R. & Mattinson, J. M., 1994. Uranium-lead zircon ages from the Median Tectonic Zone, New Zealand. *New Zealand Journal of Geology and Geophysics*, **37,** 393–419.

Kimbrough, D. L., Tulloch, A., Geary, E., Coombs, D. S. & Landis, C. A., 1993. Isotope ages from the Nelson region of South Island, New Zealand: structure and definition of the Median Tectonic Zone. *Tectonophysics*, **225,** 433–448.

Klepeis, K. A., Daczko, N. R. & Clarke, G. L., 1999. Kinematic vorticity and the tectonic significance of superposed mylonites in a major lower crustal shear zone, northern Fiordland, New Zealand. *Journal of Structural Geology*, **21,** 1385–1405.

Kohn, M. J. & Spear, F. S., 1990. Two new geobarometers for garnet amphibolites, with applications to southeastern Vermont. *American Mineralogist*, **75,** 89–96.

Konopásek, J., 1998. Formation and destabilization of the high pressure assemblage garnet-phengite-paragonite (Krusnéhory Mountains, Bohemian Massif): The significance of the Tschermak substitution in the metamorphism of pelitic rocks. *Lithos*, **42,** 269–284.

Konzett, J. & Hoinkes, G., 1996. Paragonite-hornblende assemblages and their petrological significance: an example from the Austroalpine Schneeberg Complex, Southern Tyrol, Italy. *Journal of Metamorphic Geology*, **14,** 85–101.

Koons, P. O., 1978. *Aspects of the Geology of the Southern Darran Mountains, Report G26*. New Zealand Geological Survey, City?

Landis, C. A. & Coombs, D. S., 1967. Metamorphic belts and orogenesis in southern New Zealand. *Tectonophysics*, **4,** 501–518.

Lappin, M. A. & Smith, D. C., 1978. Mantel-equilibrated orthopyroxene eclogite pods from the Basal Gneisses in the Selje District, Western Norway. *Journal of Petrology*, **19,** 530–584.

Leake, B. E., Woolley, A. R., Birch, W. D. *et al*., 1997. Nomenclature of amphiboles. *Mineralogical Magazine*, **61,** 295–321.

Marmo, B. A., Clarke, G. L. & Powell, R., 2002. Fractionation of bulk rock composition due to porphyroblast growth: effects

on eclogite facies mineral equilibria, Pam Peninsula, New Caledonia. *Journal of Metamorphic Geology*, **20,** 151–165.
Mattinson, J. L., Kimbrough, D. L. & Bradshaw, J. Y., 1986. Western Fiordland orthogneiss: Early Cretaceous arc magmatism and granulite facies metamorphism, New Zealand. *Contributions to Mineralogy and Petrology*, **92,** 383–392.
Miller, R. B., Brown, E. H., McShane, D. P. & Whitney, D. L., 1993. Intra-arc crustal loading and its tectonic implications, North Cascades crystalline core, Washington and British Columbia. *Geology*, **21,** 255–258.
Monie, P., Torres-Roldan, R. L. & Garcia, C. A., 1994. Cooling and exhumation of the western Betic Cordilleras, $^{40}Ar/^{39}Ar$ thermochronological constraints on a collapsed terrane. *Tectonophysics*, **238,** 353–379.
Mortimer, N., Tulloch, A. J., Spark, R. N., *et al*., 1999. Overview of the Median Batholith, New Zealand: a new interpretation of the geology of the Median Tectonic Zone and adjacent rocks. *Journal of African Earth Sciences*, **29,** 257–268.
Muir, R. J., Ireland, T. R., Weaver, S. D., Bradshaw, J. D., Evans, J. A., Eby, G. N. & Shelly, D., 1998. Geochronology and geochemistry of a Mesozoic magmatic arc system, Fiordland, New Zealand. *Journal of the Geological Society of London*, **155,** 1037–1053.
Muir, R. J., Weaver, S. D., Bradshaw, J. D., Eby, G. N., Evans, J. A. & Ireland, T. R., 1996. Geochemistry of the Karamea Batholith, New Zealand, and comparisons with the Lachlan Fold Belt granites of SE Australia. *Lithos*, **39,** 1–20.
Nathan, S., Thurlow, C., Warnes, P. & Zucchetto, R., 2000. *Geochronology Database for New Zealand Rocks*, 2nd edn. *1961–99, report 2000/*11, Institute of Geological and Nuclear Sciences City?
Newton, R. C. & Haselton, H. T., 1981. Thermodynamics of the garnet-plagioclase-Al_2SiO_5-quartz geobarometer. In: *Advances in Physical Geochemistry*, Vol. 1 (eds Newton, R. C., Navrotsky, A. & Woods, B. J.), pp. 131–147. Springer Verlag, New York.
Newton, R. C. & Perkins, D., 1982. Thermodynamic calibration of geobarometers based on the assemblages garnet-plagioclase-orthopyroxene-(clinopyroxene)-quartz. *American Mineralogist*, **67,** 203–222.
Oliver, G. J. H., 1977. Feldspathic hornblende and garnet granulites and associated anorthosite pegmatites from Doubtful Sound, Fiordland, New Zealand. *Contributions to Mineralogy and Petrology*, **65,** 111–121.
Perchuk, L. L. & Lavrent'eva, I. V., 1983. Experimental investigation of exchange equilibria in the system cordierite-garnet-biotite. In: *Kinetics and Equilibrium in Mineral Reactions* (ed. Saxena-Surendra, K.), pp. 199–239. Springer Verlag, New York.
Powell, R. & Holland, T. J. B., 1988. An internally consistent dataset with uncertainties and correlations: 3. Applications to geobarometry, worked examples and a computer program. *Journal of Metamorphic Geology*, **6,** 173–204.
Powell, R., Holland, T. J. B. & Worley, B., 1998. Calculating phase diagrams with Thermocalc: methods and examples. *Journal of Metamorphic Geology*, **16,** 577–588.
Sawyer, E. W., 1999. Criteria for the recognition of partial melting. *Physics and Chemistry of the Earth. Part a: Solid Earth and Geodesy*, **24,** 269–279.
Treloar, P. J., 1997. Thermal controls on early-Tertiary, short-lived, rapid regional metamorphism in the NW Himalaya, Pakistan. *Tectonophysics*, **273,** 77–104.
Tulloch, A. J., Ireland, T. R., Walker, N. W. & Kimbrough, D. L., 2000. *U-Pb zircon ages from the Milford Orthogneisses, Milford Sound, northern Fiordland: Palaeozoic igneous emplacement and Early Cretaceous metamorphism, Report, 2000/*6. Institute of Geological and Nuclear Sciences Science, City.
Tulloch, A. J. & Kimbrough, D. L., 1989. The Paparoa metamorphic core complex, New Zealand: Cretaceous extension associated with fragmentation of the Pacific margin of Gondwana. *Tectonics*, **8,** 1217–1234.
Umhoefer, P. J. & Miller, R. B., 1996. Mid-Cretaceous thrusting in the southern Coast Belt, British Columbia and Washington, after strike-slip fault reconstruction. *Tectonics*, **15,** 545–565.
Wandres, A. M., Weaver, S. D., Shelley, D. & Bradshaw, J. D., 1998. Change from calc-alkaline to adakitic magmatism recorded in the Early Cretaceous Darran Complex, Fiordland, New Zealand. *New Zealand Journal of Geology and Geophysics*, **41,** 1–14.
White, R. W. & Clarke, G. L., 1997. The role of deformation in aiding recrystallization: an example from a high-pressure shear zone, central Australia. *Journal of Petrology*, **38,** 1307–1329.
Whitney, D. L., Miller, R. B. & Paterson, S. R., 1999. *P–T–t* evidence for mechanisms of vertical tectonic motion in a contractional orogen: north-western US and Canadian Cordillera. *Journal of Metamorphic Geology*, **17,** 75–90.
Wood, B. L., 1972. Metamorphosed ultramafites and associated formations near Milford Sound, New Zealand. *New Zealand Journal of Geology and Geophysics*, **15,** 88–127.

Received 1 June 2001; revision accepted 12 August 2002.